Point-by-point responses to the reviewer's comments (reviewer's comments in blue and our reply in black)

Anonymous Referee #1

We appreciate the many thoughtful comments from the reviewer on our manuscript. Addressing all of the comments, we carefully revised the manuscript.

To our knowledge, this is the first report to significantly quantify the Arctic CO2 sink, which is the major breakthrough that warrants publication in Biogeoscicences. Both reviewers' comment is that the manuscript is technical and needs more scientific interpretation of the results. We added more comprehensive analyses and descriptions in the revised manuscript in terms of data handling (see response to comment #2), the improvement of pCO2 estimate (see response to comment #1), the methodology of the estimate (see response to comment #3), the robustness check of the result (see response to comment #3), the interannual variations in area-mean CO2 flux (see response to comment #4), and others. We also added the implication of the effect of Re, and the suggestions from our results (please see response to the reviewer #2). We are now confident that the revised manuscript has been much improved and hopefully acceptable for publication. Point-by-point responses to the reviewer's comments are given below.

General comments: The authors of this manuscript try to estimate the surface ocean partial pressure of CO2 (pCO2) distribution in the Arctic Ocean using their technique of Self-Organizing Map (SOM) and evaluated the air-sea CO2 flux. Basically, major theme of the manuscript is the improvement of the pCO2 estimate published by the authors (2016, Polar Science) in the same region by adding chlorophyll a concentration (Chl-a). I am wondering why the authors didn't plan to adopt Chl-a concentration in the previous article since the Chl-a product had already existed before. Moreover, it seems to me that the scientific insights are not sufficient on the manuscript since the estimated annual net air-sea CO2 exchange in this study is quite same with that of Yasunaka et al (2016) and it only reduced the uncertainty. At this stage, therefore, I have not any confidence that the manuscript is suitable for publication in Biogeosciences. I suggest that more careful analyses and descriptions are needed at least before re-submission of the manuscript for review.

In our first paper we did not include Chlorophyll a concentration (Chl-a) as the available products (e.g. NASA's OceanColor dataset) have several shortcomings. For example, there were a lot of missing values and large uncertainties in the Arctic area because of sea ice, low angle of sunlight, and cloud cover. In addition standard Chl-a products are

also prone to error due to the co-occurrence of high colored dissolved organic matter (CDOM) and total suspended matter (TSM) concentrations in the Arctic shelf seas (e.g., Matuoka et al., 2007; Lewis et al., 2016). In this submission we now deal with this by carefully reviewing the algorithms for extracting Chl-a from satellite remote sensing reflectance (Rrs) with the aid of an expert for the satellite color image (Eko Siswanto as the second author). As a result, three algorithms were chosen for our analysis (Section 3.1). We also carefully interpolated Chl-a so as to fit with the original data (Section 3.2). Finally, we carried out a thorough examination of the uncertainty of the obtained Chl-a values (Section 4.1). We believe that Chl-a data used in this study has much less uncertainty than standard Chl-a data for the following reasons: 1) we used local Arctic Chl-a algorithms; and 2) pixels with invalid Chl-a data due to high CDOM and TSM were discarded (before interpolation); thus 3) interpolation conducted here was only based on valid Chl-a data. Reducing uncertainty of input data (e.g., Chl-a in this study) is a prerequisite when dealing with quantitative analysis related to biogeochemical processes. We rephrased the abstract and the introduction to emphasize these points (line 35-37; line 95-103).

We consider the reduction of the uncertainty to be a substantial improvement over earlier estimates. To our knowledge, this is the first report to significantly quantify the Arctic CO2 sink and that is the major breakthrough that warrants publication in Biogeoscicences. Reducing the uncertainty of this quantification is a key contribution to the larger work of constraining the global carbon budget (e.g., Le Quere et al., 2016). Because the Arctic is an important CO2 sink, quantifying its fluxes and minimizing the uncertainty is of great scientific value. We added these statements in the revised manuscript to clarify the added value of our study (line 617-620). We additionally note that the pCO2 data set used in the present study was significantly enhanced compared to that used in previous study.

We will add more comprehensive analyses and descriptions in the revised manuscript according to, and based on, the reviewers' comments in terms of data handling, the improvement of the pCO2 estimate, the methodology of the assessment, the robustness check of the result, the interannual variations in area-mean CO2 flux, and others (see below).

Major comments: 1) Although the authors mentioned that the addition of Chl-a as a parameter in the SOM process enabled them to improve the estimate of pCO2 via better representation of its decline in spring (I think the authors mentioned about the lower panels of the figure 11), it seems that the pCO2 variation estimated with Chl-a in the

observed regions was similar to that without Chl-a especially from spring to fall (upper panels of the figure 11). I suggest the authors show further evidences that pCO2 estimate with Chl-a improved the pCO2 variation in spring better (for example, monthly RMSD variations with Chl-a/without Chl-a, etc).

We present the difference in bias and RMSD for pCO2 estimated with and without Chl-a; Figure A shows the time-evolution and Figure B shows the spatial distribution. pCO2 estimates in winter tend to be low and those in summer tend to be high, and the systematic biases and RMSDs are suppressed in the estimates with Chl-a in both seasons (Figure A). Biases and RMSDs are reduced in the Canada basin, the western Bering Sea, and the boundary region between the Norwegian Sea and the subpolar North Atlantic (Figure B). It means the strong east–west contrast in the Bering Sea and the contrast between the Canada Basin and the Chukchi Sea (see Figure 4) were better represented in the estimates with Chl-a. That is, including Chl-a when estimating pCO2 yields not only better representation of the pCO2 decline in spring to summer season but also better representation of the contrast in time and in space. We added these results to the revised manuscript (line 577-596; Fig. S1; Fig. S2).

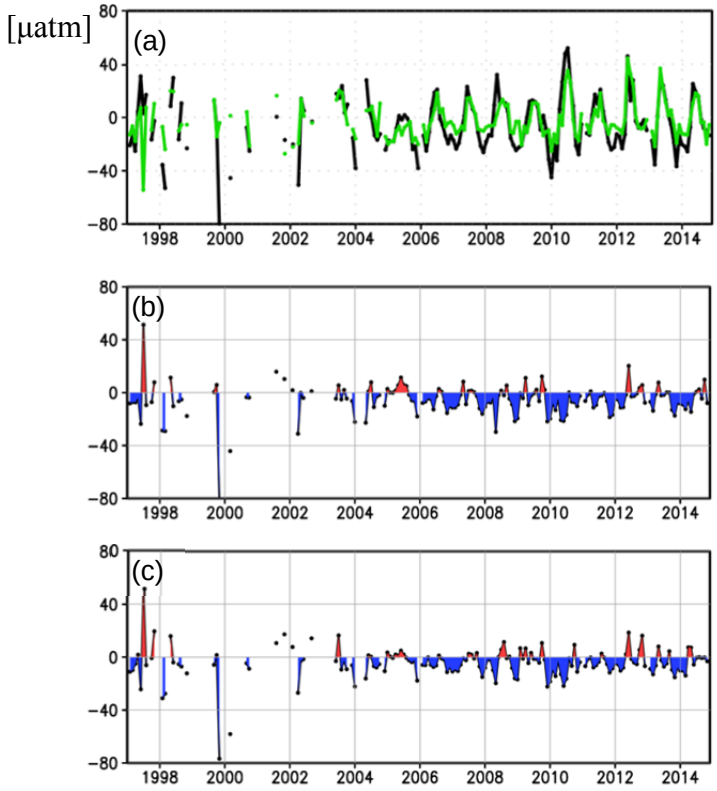

Figure A: (a) pCO2 bias (estimate – observation) averaged over the entire analysis area [µatm], for the estimates with Chl-a (green) and without Chl-a (black). Difference in (b) absolute bias and (c) RMSD for pCO2 estimated with and without Chl-a averaged over

the entire analysis area [µatm]. Negative value means improvement of the estimates in b and c.

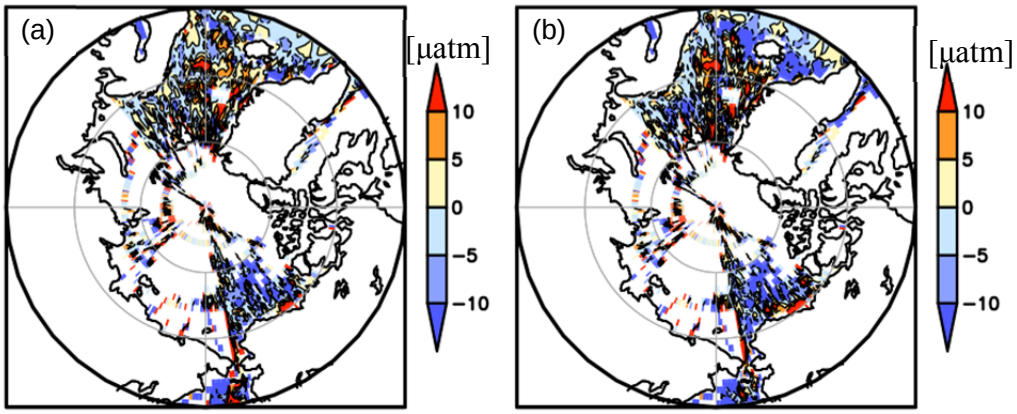

Figure B: Difference in (a) absolute bias and (b) RMSD for pCO2 estimated with and without Chl-a averaged over the whole analysis period [µatm]. Negative value means improvement of the estimates.

2) I am not comfortable with the author's data handlings. First, the combination data of "non-public" JAMSTEC pCO2 data with "public" SOCAT and LDEO data seems to be bit unfair since no one can't get the same results even if they use the public datasets. To guarantee the fairness, the authors should mention that the JAMSTEC data used in this study would be submitted to SOCAT and/or LDEO database soon. Second, I could not understand why the authors executed the data selection described in Lines 220-225 while the SOCAT and LDEO datasets had been already quality-controlled by researchers. I agree that the data selection may be needed for non-quality-controlled data such as nutrient recorded in the World Ocean Database, but I think it is unnecessary in pCO2. I am seriously concerned that the data selection in this work (and in previous work) might affect the apparent uncertainty in the pCO2 estimate and the evaluated RMSD was underestimated. Third, the authors used DIC data from the upper 30 m if there were no samples from above 10 m. I think the use of the data close to 30 m needs to be more careful treatment especially in summer, when the mixed layer depth is likely shallower than the sampling depth. I suggest that a comparison between observed pCO2 or calculated pCO2 from DIC samples shallower than 10 m and calculated pCO2 deeper than 10 m would be needed for examining the availability.

JAMSTEC pCO2 data are publicly available through the JAMSTEC web site (http://www.godac.jamstec.go.jp/darwin/e). We have additionally encouraged the PIs of these data to submit them to the SOCAT and LDEO database.

As the reviewer mentioned, pCO2 data in the SOCAT and LDEO database have been quality-controlled. These may well be realistic values, but are often extreme values reflecting the small spatial scale and/or short time scale variations that can be quite different from the large-scale variability of interest in this study. Therefore, to limit the possibility of biasing the results with small scale and short-term variability, we decided to conduct the additional quality control to exclude outliers not representative of the basin-wide distribution. We rephrased this description in the revised manuscript (line 255-259; line 269-271).

Above 10m depth there are 1795 data, in the 10-20m range there are 296, and in the 20-30m range 75. We checked the difference between directly measured pCO2 and calculated pCO2 using the data at cruises where both underway pCO2 and bottle DIC/TA samples are available (10% of the bottle samples, i.e., 245 pairs). Measured and calculated pCO2 values are 289 ± 11 μatm and 299 ± 41 μatm, respectively. The mean values are slightly lower for measured pCO2 values than for calculated ones, but the difference is smaller than the standard deviation and the uncertainties of the calculation (the latter of which is 14 μatm; Lueker et al., 2000). The difference between measured and calculated pCO2 is not dependent on the depth where the TA/DIC samples were obtained – note that the observed pCO2 values are generally from 4–6m. Calculated pCO2 values above 10m are 288 ± 11 μatm and 298 ± 43 μatm, and those in the 10–30m range are 294 ± 9 μatm and 302 ± 36μatm. We added these results to the revised manuscript (line 137-139; line 144-155).

3) I found both the manuscript and the article of Yasunaka et al. (2016) adopted atmospheric xCO2 as one of the training parameters to reconstruct oceanic pCO2 trend. Since Yasunaka et al. (2016) seemed to adopt xCO2 to estimate pCO2 in the SOM process for the first time, I also read the article. Consequently, I was bit disappointed there was not any descriptions of effectivity and validation by adopting xCO2 and found only the sentence in the manuscript that "We believe that this (adopting xCO2) better represents the real variability and trends of pCO2w.", which is not reasonable explanation. Moreover, based on my thoughts, SOM technique may be rather unsuitable to reconstruct pCO2 trend while other techniques such as feed-forward neural network are suitable for it. The reason is that each neuron in the SOM has only one pCO2 value. As the authors know, neurons are classified in accordance with the variations of

respective parameters (X, Y, SST, Salinity, Chl-a, SIC, xCO2 in this study) at the training process and most of them are labelled by the respective pCO2 values at the labeling process. For example, when the temporal pCO2 distribution is weighted toward later period like in this study, many of neurons tend to be labelled by the pCO2 values which were observed in the later period. In that case, though the estimated spatial-mean temporal pCO2 variations in the region where the observations had been made showed good agreement with measurements as shown in figures 4 and 5, it may be seen that the pCO2 value observed in the later period is likely assigned to the grid at the former period where the pCO2 measurements have not been made. To clear my doubts, I would suggest that the authors show the temporal variations for 18 years in the respective regions including the region where a few/no observations have not been made in the manuscript and discuss the trends.

According to the inter-comparison study by Rodenbeck et al. (2015), the pCO2 trends estimated by feed-forward networks and by SOM agreed quite well. To represent the anthropogenic pCO2 increase, several previous studies have assumed a homogeneous and monotonic increase in the whole analysis area (Nakaoka et al. 2013; Zheng et al. 2014). They subtracted the trend before the estimate and recombined it after the estimate. But a monotonic increase has not been assured. Actually, the spatial pattern of the pCO2 trend (see Figure Ca) is far from homogeneous. Instead of that, we included atmospheric xCO2 as a training parameter following Landschutzer et al. (2013, 2014). We added text about these points in the revised manuscript (line 285-293).

As the reviewer mentioned, the pCO2 values observed in the latter period may be used for the pCO2 estimate in the former period. To validate our estimated pCO2 values for periods and regions without any observed data, we repeated the mapping experiments after systematically excluding some of the observed pCO2 data when labeling the neurons; four experiments were carried out, by excluding data (1) for 1997–2004, (2) for January to April, (3) from north of 80°N, and (4) from the Laptev Sea (90°E – 150°E), where there are only a few pCO2 observations. We compared the pCO2 estimates obtained in each experiment with the excluded observations and found that the pCO2 estimates reproduced the general features of the observed spatial distribution and temporal variation. They were also similar to the pCO2 estimates obtained by using all observations, although RMSDs between the estimates and the excluded observations are 1.8 times the RMSDs of the estimates based on all observations as mentioned in Section 4.2. It means that our estimated pCO2 would reproduce the general features both in space and time even when and where there are no observed data. We rephrased the relevant text in the revised manuscript (line 407-422).

According to the reviewer's suggestion, we examined the correspondence between pCO2 trend and the year when the first observation was made in each grid point (Figure C). Spatial distribution of pCO2 trend did not correspond to the year when the first observation was made. We also checked the pCO2 interannual variation and the year of observed in the several regions. Here we show them in 73–77°N 175°E –175°W, 73–77°N 160–150°W, and 73–77°N 135–125°W where the trend and the observed year are different separating only several degrees in longitude (Figure D). The pCO2 trends increase from west to east, while the observational data are from 2004 in the west, from 1999 in the middle, and from 2011 in the east. It shows again the amplitudes of trend do not correspond the year when the first observation was conducted. We added these descriptions in the revised manuscript (line 562-568; Supplement).

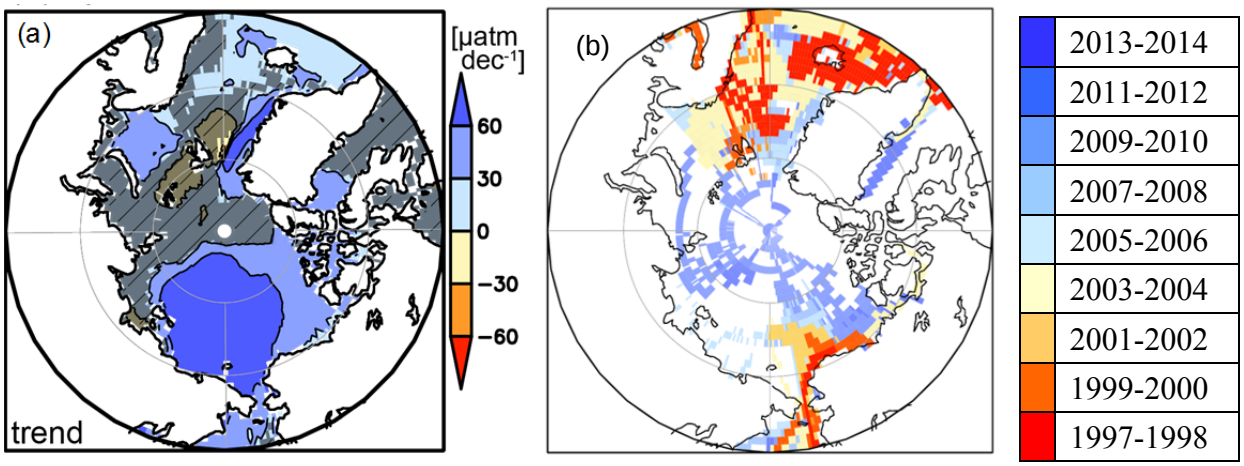

Figure C: (a) pCO2 trend. Darker hatched areas represent values in grids where trend values were less than the uncertainty. (b) Year when the first observation was retained.

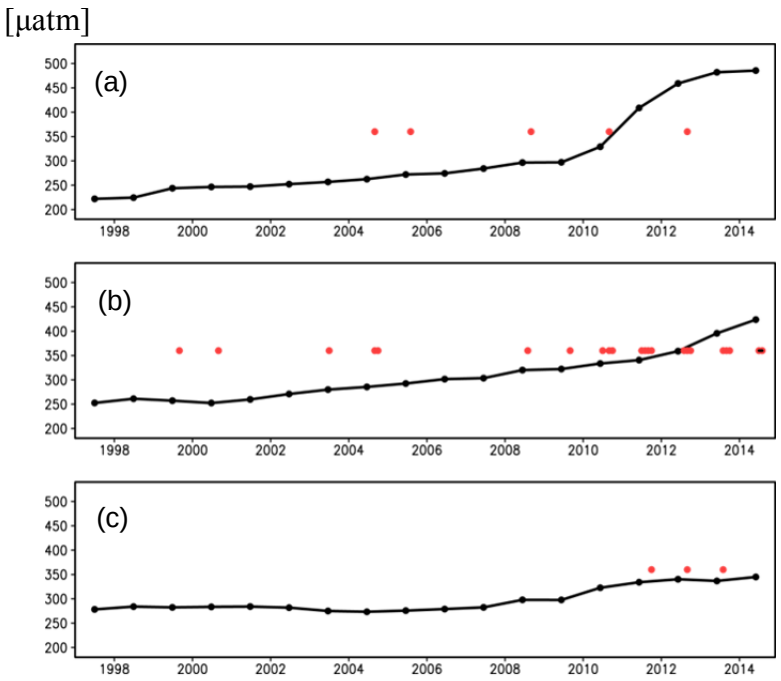

Figure D: The pCO2 interannual variation and the year of observed in (a) 73–77°N 175°E –175°W, (b) 73–77°N 160–150°W, and (c) 73–77°N 135–125°W.

4) I am wondering why the authors didn't examine the temporal variation of air-sea CO2 exchange and its relevant factors in the whole of the Arctic Ocean. I think those might make the manuscript more suggestive one to understand whether the oceanic CO2 uptake will increase or decrease in the region as global warming progresses, even if the estimated budget has large uncertainty.

We agree the reviewer's comment, and added a figure of the CO2 flux in several regions of the Arctic Ocean and some text explaining that in the revised manuscript (line 539-555; Fig. 11). Figure E shows interannual variation of CO2 flux and related variables in several regions. In the Greenland/Norwegian Sea, interannual variation of the CO2 flux negatively correlates with the wind speed (CO2 influx to the ocean is large when the wind is strong; correlation coefficient R = –0.41), while ΔpCO2 and sea ice change is small. In the Barents Sea, interannual variation of CO2 flux negatively correlates with the sea ice concentration (R = –0.50), while correlation with wind speed is not significant and ΔpCO2 change is small. In the Chukchi Sea, CO2 influx to ocean is decreasing with the increasing ΔpCO2 (R = 0.87); high pCO_{2w} (>500 µatm) has been sometimes observed in the Chukchi Sea after 2010 (Hauri et al. 2013). The interannual variability of the CO2 flux averaged over the Arctic Ocean is small because the increasing ΔpCO2 seems to be compensated by the effect of sea ice retreat (R = –0.70).

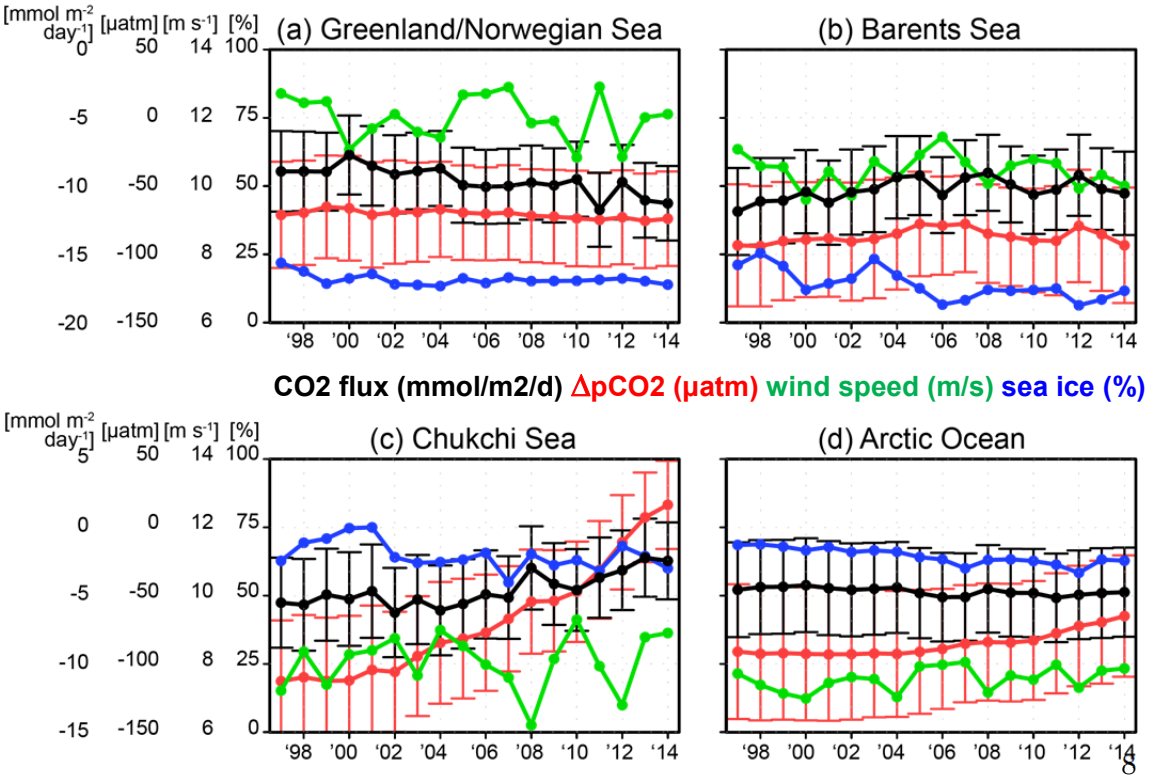

Figure E: Time evolution of the air-sea CO2 flux and its driving factors in (a) the Greenland/Norwegian Seas, (b) the Barents Sea, (c) the Chukchi Sea and (d) the Arctic Ocean.

Specific comments: Lines 99-103: While SOCAT publishes the data as fugacity of CO2 (fCO2), LDEO opens the data as pCO2. Did the authors treat the fCO2 and pCO2 data as they are (without any correction)?

We converted SOCAT fCO2 values to pCO2 values, and then combined these with the LDEO pCO2 values. This was clarified in the revised manuscript (line 116-123).

Line 324: The description of figure 4c is presented after those of figures 5a and 5b. It would be better to fix this.

We agree. We combined Figures 4 and 5 of the previous manuscript, and change the order (Figs. 4 and 5 of the revised manuscript).

Line 382: The description of figure 7 is presented before those of figures 6c and 6d. It would be better to fix this.

We agree. We extracted Figures 6c and 6d of the previous manuscript into a separate figure, and put them after Figure 7 (Fig. 8 of the revised manuscript).

Line 387: The description of figure 6d is presented before that of figures 6c. It should fix it.

The reviewer is right. We changed the order (Fig. 8 of the revised manuscript).

Lines 483-484: Is there any plan to open the pCO2 data in the website?

We plan to make public the pCO2 data and the interpolated Chl-a data by this study on the same website. We added the information to the revised manuscript (line 667-669).

Minor comment: Line 256: Telzewski et al. should change to Telszewski et al.

The reviewer is right. We corrected this (line 308).

Anonymous Referee #2

Reviewer comment: The authors present an improved version of the Yasunaka et al. (2016) estimate of the uptake of CO2 by the Arctic Ocean. The paper is very clearly written and the detail in quantifying uncertainty is impressive. The principal limitation

of the manuscript is that it is very technical, and will likely need to touch more closely and directly on broader scientific questions to be recommended for publication in Biogeosciences. In my opinion, this could be accomplished with minor revisions, consisting of adding to the Conclusions with a few paragraphs and emphasizing the broader implications and relevance for identifying key processes and/or optimization observing system design.

We appreciate the positive evaluation and helpful comments from the reviewer. Referring to the comments, we carefully revised the manuscript. Both reviewers' comment is that the manuscript is technical and needs more scientific interpretation of the results. We added descriptions in the revised manuscript about the improvement of our pCO2 estimate (see response to the first minor point), the interannual variations in area-mean CO2 flux (see response to the first main point), the effect of Re (see response to the second minor point), and the scientific implications of our results (see response to the first and second main points). We also added the analyses and descriptions about data handling, the improvement of pCO2 estimate by the Chl-a, the methodology of the assessment, and the robustness check of the result (please see response to the reviewer #1). Point-by-point responses to the reviewer's comments are given below.

Main Points: Although the authors have done a very good job of quantifying uncertainty in pCO2 and air-sea CO2 fluxes, the paper would benefit from commentary on the implications for optimization of the observing network. The other missing component of the study is a mechanistic interpretation of the main results, perhaps as part of the Conclusions. In the Introduction, there is a broad overview of the mechanisms that might impact trends in carbon fluxes over the Arctic, but it was surprising that these points did not get addressed in the Conclusions.

There are still too few observations in the Kara Sea, the Laptev Sea, the East Siberian Sea and the Eurasian Basin to determine seasonal and interannual variations with great reliance there. To improve our understanding of the variability in air–sea CO_2 fluxes in the Arctic, it is therefore of critical importance to obtain additional ocean CO_2 measurements to fill these data gaps, and that these measurements are made publically available. Data synthesis activities like SOCAT must be encouraged. We added these points to the revised manuscript (line 623-630).

The reviewer makes a good point, and we added a figure and additional description of the interannual variations in area-mean CO2 flux in the revised manuscript (line 539-555; Fig. 11). In the Greenland/Norwegian Sea, interannual variation of the CO2 flux negatively correlates with the wind speed (CO2 influx to the ocean is large when

the wind is strong), while ΔpCO2 and sea ice change are small. In the Barents Sea, interannual variation of the CO2 flux negatively correlates with the sea ice concentration, while correlation with wind speed is not significant and ΔpCO2 change is small. In the Chukchi Sea, CO2 influx to the ocean is decreasing with the increasing ΔpCO2; high pCO_{2w} (>500 μatm) has been observed in the Chukchi Sea after 2010 (Hauri et al. 2013). Interannual variability of CO2 flux averaged over the entire Arctic Ocean is small because increasing ΔpCO2 compensates for the sea ice retreat.

Given the availability of forward ocean biogeochemistry models that include the Arctic, I believe that the burden on the authors to provide at the very least an account of why they do not consider an Observing System Simulation Experiment (OSSE) to assess the skill of their method. Presumably some of the models that participate in the Global Carbon Project are open-access, and could be sampled with the spatial/temporal coordinates of the SOCAT and other pertinent data products? If the authors have scientific reasons for not finding the process-representation of the current generation of models to be up to the task, what then are the critical scales and processes that would be critical to represent?

We agree that the assessment of our estimate using numerical models or their outputs would likely be useful. Conversely, assessment of the numerical models using our estimate of Arctic carbon uptake is also an interesting topic since numerical models are poorly validated in the Arctic due to the limited observations of biogeochemistry. However, such experiments need thorough insight into the numerical models, which is beyond the scope of this study. We hope to perform such comparisons in future studies. Instead, in the present study, we assessed the accuracy of our estimate by systematically excluding some of the observed pCO2 data when labeling the neurons (section 4.2). We added the descriptions in the revised manuscript (line 662-666).

Minor Points: It would be good if the authors could point out whether there are important methodological differences between their method and others in the literature that use neural-network-type approaches.

This is a nice recommendation from the reviewer and we added a description of the major differences in the revised manuscript (line 294-297). Instead of the normalization of pCO2 to the reference year, we used atmospheric xCO2 as a training parameter. To avoid intricately intermingled estimates in space and time in regions and seasons with limited CO2 observations, we added geographical position to the set of training parameters: X = sin(latitude) × cos(longitude) and Y = sin(latitude) × sin(longitude). On

the other hand, we did not use mixed layer depth because of lack of reliable data in the Arctic.

The Revelle factor was mentioned in the Introduction, and it would be very helpful to know if the authors believe that this will be an important factor over the Arctic when considering future climate change. It would be useful to discuss this as it pertains to the transient signal, and whether there is evidence that it is more important here than in other subpolar or circumpolar regions.

Revelle factor (Re), (ΔpCO2 / pCO2) / (ΔDIC / DIC), is a measure of the amount of CO2 which a parcel of seawater can dissolve for a given increase in pCO2. Summer time Arctic surface waters (70–80°N) have high Re of about 18, whereas the summer Irminger Sea surface waters (~64°N) in the northern North Atlantic have about 12 and a global ocean mean is about 10 (Takahashi, personal communication). The high Re is a result of the reduced salinity, which is maintained by the strong vertical density gradients below the low salinity surface layer reducing vertical mixing of high salinity deep waters. Higher Re values indicate that a given mass of seawater can absorb less CO2 in response to increasing atmospheric CO2. This means that the Arctic surface waters have small absorbing capacity for atmospheric CO2 even though surface water pCO2 is low.

Re will also be of importance for the changing Arctic as it is a function of temperature and salinity, both which are believed to change in the future. In specific, warmer temperature will lead to a decrease in Re (an increase in buffering capacity) while lower salinity will have the opposite effect and cause an increase Re. Given the future Arctic Ocean is warming and freshening, the net effect is unclear but would be small. In our current study, we used climatological-mean salinity for the pCO2 estimate because of lack of reliable year-to-year salinity data. That might be one of the improvement points for a future study.

Other complicating effects, such as the increasing input into the Arctic Ocean of river water (of higher alkalinity than river input into most other oceans), are also interesting topics, but not in the scope of the present study. We added these points in the concluding section of the revised manuscript (line 631-637).

Arctic Ocean CO_2 uptake: an improved multi-year estimate of the air–sea CO_2 flux incorporating chlorophyll-a concentrations

Sayaka Yasunaka[1,2], Eko Siswanto[1], Are Olsen[3], Mario Hoppema[4], Eiji Watanabe[2], Agneta Fransson[5], Melissa Chierici[6], Akihiko Murata[1,2], Siv K. Lauvset[3,7], Rik Wanninkhof[8], Taro Takahashi[9], Naohiro Kosugi[10], Abdirahman M. Omar[7], Steven van Heuven[11], and Jeremy T. Mathis[12]

[1]Research and Development Center for Global Change, Japan Agency for Marine-Earth Science and Technology, Yokosuka, Japan

[2]Institute of Arctic Climate and Environment Research, Japan Agency for Marine-Earth Science and Technology, Yokosuka, Japan

[3]Geophysical Institute, University of Bergen and Bjerknes Centre for Climate Research, Bergen, Norway

[4]Alfred Wegener Institute Helmholtz Centre for Polar and Marine Research, Climate Sciences Department, Bremerhaven, Germany

[5]Norwegian Polar Institute, Fram Centre, Norway

[6]Institute of Marine Research, Tromsø, Norway

[7]Uni Research Climate, Bjerknes Centre for Climate Research, Bergen, Norway

[8] National Oceanic and Atmospheric Administration, Atlantic Oceanographic and Meteorological Laboratory, Miami, FL, USA

[9]Lamont-Doherty Earth Observatory of Columbia University, Palisades, NY, USA

[10]Oceanography and Geochemistry Research Department, Meteorological Research Institute, Japan Meteorological Agency, Tsukuba, Japan

[11]Energy and Sustainability Research Institute Groningen, Groningen University, The Netherlands

[12] National Oceanic and Atmospheric Administration, Arctic Research Program, Seattle, WA, USA

Abstract

We estimated monthly air–sea CO_2 fluxes in the Arctic Ocean and its adjacent seas north of 60° N from 1997 to 2014. This was done by mapping partial pressure of CO_2 in the surface water (pCO_{2w}) using a self-organizing map (SOM) technique incorporating chlorophyll-a concentration (Chl-a), sea surface temperature, sea surface salinity, sea ice concentration, atmospheric CO_2 mixing ratio, and geographical position. We applied new algorithms for extracting Chl-a from satellite remote sensing reflectance with close

examination of uncertainty of the obtained Chl-a values. The overall relationship between pCO_{2w} and Chl-a was negative, whereas the relationship varied among seasons and regions. The addition of Chl-a as a parameter in the SOM process enabled us to improve the estimate of pCO_{2w} particularly via better representation of its decline in spring which resulted from biologically mediated pCO_{2w} reduction. As a result of the inclusion of Chl-a, the uncertainty in the CO_2 flux estimate was reduced, with a net annual Arctic Ocean CO_2 uptake of 180 ± 130 TgC y^{-1}. Seasonal to interannual variation of the CO_2 influx was also figured out.

1. Introduction

The Arctic Ocean and its adjacent seas (Fig. 1) generally act as a sink for atmospheric CO_2 because of the high solubility of CO_2 in their low-temperature waters, combined with extensive primary production during the summer season (Bates and Mathis, 2009). The Arctic Ocean and its adjacent seas consist of complicated subregions that include continental shelves, central basins, and sea-ice-covered areas. Therefore, the surface partial pressure of CO_2 (pCO_{2w}) distribution is not only affected by ocean heat loss and gain, and biological production and respiration, but also by sea-ice formation and melting, river discharge, and shelf–basin interactions (cf. Bates and Mathis, 2009, and

references therein). However, CO_2 measurements are sparse in this very heterogeneous area (Fig. 2), and hence the existing air–sea CO_2 flux estimates in the Arctic are poorly constrained (Bates and Mathis, 2009; Schuster et al., 2013; Yasanuka et al., 2016).

As global warming progresses, melting of sea ice will increase the area of open water and enhance the potential for atmospheric CO_2 uptake (e.g., Bates et al., 2006; Gao et al., 2012). However, other processes could suppress CO_2 uptake. For example, increasing seawater temperatures, declining buffer capacity due to the freshening of Arctic surface water by increased river runoff and melting of sea-ice, and increased vertical mixing supplying high-CO_2 water to the surface will all result in a tendency for reduced uptake (Bates and Mathis, 2009; Cai et al., 2010; Chierici et al., 2011; Else et al., 2013; Bates et al. 2014; Fransson et al., 2017). The combined effect of all these processes on ocean CO_2 uptake has not yet been clarified for the Arctic.

Yasunaka et al. (2016) prepared monthly maps of air–sea CO_2 fluxes from 1997 to 2013 for the Arctic north of 60° N by applying, for the first time, a self-organizing map (SOM) technique to map pCO_{2w} in the Arctic Ocean. The advantage of the SOM technique is its ability to empirically determine relationships among variables without making any a priori assumptions (about what types of regression functions are applicable, and for which sub-regions the same regression function can be adopted, for

example). The SOM technique has been shown to reproduce the distribution of pCO_{2w} from unevenly distributed observations better than multiple regression methods (Lefèvre et al., 2005; Telszewski et al., 2009). The uncertainty of the CO_2 flux estimated by Yasunaka et al. (2016), however, was large (±3.4–4.6 mmol m^{-2} d^{-1}), and the estimated CO_2 uptake in the Arctic Ocean was smaller than the uncertainty (180 ± 210 TgC y^{-1}). One possible reason for the large uncertainties is that no direct proxies for the effect of biological processes on pCO_{2w} were used in that study, leading to an underestimation of the seasonal amplitude of pCO_{2w}.

Remotely sensed chlorophyll-a concentrations (Chl-a) has been used in several pCO_{2w} mapping efforts as a direct proxy for the effect of primary production. For example Chierici et al. (2009) produced pCO_{2w} algorithms for the subpolar North Atlantic during the period from May to October and found that the inclusion of Chl-a improved the fit substantially. Measurements in several areas of the Arctic show that relationships between pCO_{2w} and Chl-a occur also in this region. They correlate negatively (Gao et al., 2012; Ulfsbo et al., 2014), as expected from the drawdown of CO_2 during photosynthesis, but exceptions do occur; in coastal regions the correlation is positive (Mucci et al., 2010).

Several studies have demonstrated that Chl-a in the Arctic can be estimated from

satellite remote sensing reflectance (Rrs) (e.g. Arrigo and Dijken, 2004; Cota et al., 2004). Perrette et al. (2011) showed that satellite-derived Chl-a successfully captured a phytoplankton bloom in the ice-edge region. Changes in the seasonal cycle from a single peak to a double peak of Chl-a have also been detected and are likely a consequence of the recent sea-ice loss in the Arctic (Ardyna et al., 2014). However, the available products (e.g. NASA's OceanColor dataset) in the Arctic include large uncertainty and many missing values because of sea ice, low angle of sun-light and cloud cover, and are also prone to error due to the co-occurrence of large colored dissolved organic matter (CDOM) and total suspended matter (TSM) concentrations (e.g., Matuoka et al., 2007; Lewis et al., 2016). Here we deal with these issues by using several Chl-a algorithms optimised for the Arctic and others, and by excluding Chl-a data from grid cells potentially affected by CDOM and TSM. Calculated Chl-a values were then interpolated Chl-a so as to fit with the original data. Using these data, we examined the relationship between pCO_{2w} and Chl-a in the Arctic Ocean and its adjacent seas, and computed monthly air–sea CO_2 flux maps for regions north of 60° N using a SOM technique similar to that of Yasunaka et al. (2016), and with Chl-a added to the SOM process.

2. Data

2.1. $pCO_{2\,w}$ measurements

We used fugacity of CO_2 (fCO_{2w}) observations from the Surface Ocean CO_2 Atlas version 4 (SOCATv4; Bakker et al., 2016; http://www.socat.info/; 1,983,799 data points from >60° N), and pCO_{2w} observations from the Global Surface pCO_2 Database Version 2014 (LDEOv2014; Takahashi et al., 2015; http://cdiac.ornl.gov/oceans/LDEO_Underway_Database/; 302,150 data points from >60° N). In the LDEO database, pCO_{2w} is based on measured CO_2 mixing ratio in a parcel of air equilibrated with sea-water sample, and computed assuming CO_2 as an ideal gas, whereas in the SOCAT, fCO_2 is obtained considering the non-ideality from CO_2-CO_2 and CO_2-H_2O molecular interactions. Because of ambiguities in the CO_2-H_2O interaction corrections, the SOCAT fCO_{2w} values are converted to pCO_{2w} values (a correction of <1 %), and then combined them with the LDEO pCO_{2w} values. When data points were duplicated in the SOCAT and LDEO datasets, the SOCAT version was used, except for the data obtained from onboard the USCGC *Healy* as these have been reanalyzed by Takahashi et al. (2015). Altogether 200,409 duplicates were removed. We also used shipboard pCO_{2w} data obtained during cruises of the R/V *Mirai* of the Japan Agency for Marine-Earth Science and Technology (JAMSTEC) that have not yet been

included in SOCATv4 or LDEOv2014 (cruises MR09_03, MR10_05, MR12_E03, and MR13_06; available at http://www.godac.jamstec.go.jp/darwin/e; 95,725 data points from >60° N). In total, we used 2,181,265 pCO_{2w} data points, 33 % more than used by Yasunaka et al. (2016).

To further improve the data coverage, especially for the ice-covered regions, we also used 2166 pCO_{2w} values calculated from dissolved inorganic carbon (DIC) and total alkalinity (TA) data extracted from the Global Ocean Data Analysis Project version 2 (GLODAPv2; Key et al., 2015; Olsen et al., 2016; http://www.glodap.info). 90% of these data were obtained at cruises without underway pCO_{2w} data. We extracted values of samples obtained from water depths shallower than 10 m, or the shallowest values from the upper 30 m of each cast if there were no values from above 10 m. There are 1795 data points above 10 m depth, 296 in the 10–20 m range, and 75 in the 20–30 m range. This resulted in 94 % more calculated pCO_{2w} values than used by Yasunaka et al. (2016), and altogether the number of directly measured and calculated data points used here is 33% more than used in Yasunaka et al. (2016). The CO2SYS program (Lewis and Wallace, 1998; van Heuven et al., 2009) was used for the calculation with the dissociation constants reported by Lueker et al. (2000) and Dickson (1990).

We checked the difference between calculated pCO_{2w} and measured pCO_{2w} using the

data from cruises with both bottle DIC/TA samples and underway pCO_{2w} available (10% of the bottle samples, i.e., 245 pairs). Mean value for the calculated pCO_{2w} values from bottle DIC/TA samples from the upper 30 m was 299 ± 42 µatm, and that for the corresponding directly measured pCO_{2w} values from underway observation generally at 4–6m was 289 ± 11 µatm. The mean values are slightly higher for calculated pCO_{2w} values than for measured ones, but the difference is smaller than the standard deviation and the uncertainties of the calculation (the latter of which is 14 µatm; see Section 4.2). The difference between calculated and measured pCO_{2w} is not dependent on the depth where the TA/DIC samples were obtained. It was 10 ± 31 µatm for samples from above 10 m, 7 ± 27 µatm for samples from 10–20 m, and 11 ± 47 µatm for samples from 20–30 m.

The availability of pCO_{2w} data (measured and calculated) varies spatially and temporally (Fig. 2). Most of the available data are from the subpolar North Atlantic, the Greenland Sea, the Norwegian Sea, the Barents Sea, and the Chukchi Sea while much less data are available for the Kara Sea, the Laptev Sea, the East Siberian Sea, and the Eurasian Basin. The number of pCO_{2w} data increased after 2005, but there are also a substantial number of data from before 2004.

2.2. Other data

To calculate Chl-a, we used merged Rrs data from the SeaWiFS, MODIS-Aqua, MERIS, and VIIRS ocean color sensors processed and distributed by the GlobColour Project (Maritorena et al., 2010; http://hermes.acri.fr/index.php?class=archive). For compatibility with the spatio-temporal resolution of the gridded pCO_{2w} data (see below Sect. 3.3), we selected monthly mean Rrs data with a spatial resolution of 1° (latitude) × 1° (longitude).

Sea surface temperature (SST) data were extracted from the National Oceanic and Atmospheric Administration (NOAA) Optimum Interpolation SST Version 2 (Reynolds et al., 2002; http://www.esrl.noaa.gov/psd/data/gridded/data.noaa.oisst.v2.html). These data are provided at a resolution of 1° × 1° × 1 month. Sea surface salinity (SSS) data were retrieved from the Polar Science Center Hydrographic Climatology version 3.0, which also has a resolution of 1° × 1°× 1 month (Steele et al., 2001; http://psc.apl.washington.edu/nonwp_projects/PHC/Climatology.html). Sea ice concentration (SIC) data were obtained from the NOAA/National Snow and Ice Data Center Climate Data Record of Passive Microwave Sea Ice Concentration version 2, which has a resolution of 25 km × 25 km × 1 month (Meier et al., 2013; http://nsidc.org/data/G02202). These data were averaged into 1° × 1° × 1 month

grid-cells. Zonal mean data for the atmospheric CO_2 mixing ratio (xCO_{2a}) were retrieved from the NOAA Greenhouse Gas Marine Boundary Layer Reference data product (Conway et al., 1994; http://www.esrl.noaa.gov/gmd/ccgg/mbl/index.html) and were interpolated into 1° × 1° × 1 month grid-cells. Both sea level pressure and 6-hourly 10-m wind speeds data were obtained from the U.S. National Centers for Environmental Prediction–Department of Energy Reanalysis 2 (NCEP 2) (Kanamitsu et al., 2002; http://www.esrl.noaa.gov/psd/data/gridded/data.ncep.reanalysis2.html). We also used the 6-hourly 10-m wind speeds from the U.S. National Centers for Atmospheric Prediction and the National Center for Atmospheric Research Reanalysis 1 (NCEP1) (Kalnay et al., 1996; https://www.esrl.noaa.gov/psd/data/gridded/data.ncep.reanalysis.html) when the gas transfer velocity was optimized for NCEP2 wind (see Section 3.5 below).

Surface nitrate measurements were extracted from GLODAPv2 (Key et al., 2015; Olsen et al., 2016) and the World Ocean Database 2013 (WOD; Boyer et al., 2013). When data points were duplicated in the GLODAPv2 and WOD datasets, the GLODAPv2 version was used as this has been subjected to more extensive quality control.

3. Methods

3.1. Calculation of chlorophyll-a concentrations

Chl-a was calculated from Rrs by using the Arctic algorithm developed by Cota et al. (2004). Several assessments have shown that this algorithm has a large uncertainty (e.g., Matsuoka et al., 2007; Lewis et al., 2016), and therefore the sensitivity of our results to this choice was evaluated by using two alternative algorithms for Chl-a: the standard algorithm of O'Reilly et al. (1998), and the coastal algorithm, of Tassan (1994).

To ensure that we were working with Rrs data relatively unaffected by CDOM and TSM, the Chl-a data were masked following the method of Siswanto et al. (2013). Briefly, the Rrs spectral slope between 412 and 555 nm ($Rrs_{555\text{-}412\ slope}$; $sr^{-1}\ nm^{-1}$) was plotted against logarithmically transformed Chl-a. Based on the scatter plot of log(Chl-a) and $Rrs_{555\text{-}412\ slope}$, we then defined a boundary line separating phytoplankton-dominated grid-cells ($Rrs_{555\text{-}412\ slope}$ < boundary value) from potentially non-phytoplankton-dominated grid-cells ($Rrs_{555\text{-}412\ slope} \geq$ boundary value) by:

$$Rrs_{555\text{-}412\ slope} = -0.000003\{\log(\text{Chl-a})\}^2 + 0.00002\{\log(\text{Chl-a})\} + 0.00006. \quad (1)$$

Grid-cells were considered invalid and masked out if 1) $Rrs_{555\text{-}412\ slope} \geq$ boundary value,

or 2) Rrs at 555nm (Rrs_{555}) > 0.01 sr^{-1} (or normalized water-leaving radiance > 2 mW cm^{-2} μm^{-1} sr^{-1}; see Siswanto et al., 2011 and Moore et al., 2012). This criterion masked 2% of all Chl-a data.

The criteria described in the previous paragraph could mask out grid-cells having coccolithophore blooms, which are sometimes observed in the Arctic Ocean (e.g., Smyth et al., 2004), as they also have Rrs_{555} > 0.01 sr^{-1} (Moore et al., 2012). Unlike waters dominated by non-phytoplankton particles, whose Rrs spectral shape peaks at 555 nm, the Rrs spectral shape of waters with coccolithophore blooms peaks at 490 or 510 nm (see Iida et al., 2002; Moore et al., 2012). Therefore, grid-cells with Rrs spectral peaks at 490 or 510 nm (already classified using the criteria of Rrs at 490nm (Rrs_{490}) > Rrs at 443nm (Rrs_{443}) and Rrs at 510nm (Rrs_{510}) > Rrs_{555}) were considered as coccolithophore grid-cells, and were reintroduced. 8% of the masked Chl-a data were reintroduced by this criterion.

3.2. Chlorophyll-a interpolation

Chl-a values are often missing because of cloud cover, low angle of sunlight, or sea ice. For the period and area analyzed here, data are missing for 86 % of the space and time grid-cells. Because pCO_{2w} mapping requires a complete Chl-a field without missing

values, we interpolated the Chl-a data as follows; 1) Chl-a was set to 0.01 mg m^{-3} (minimum value of Chl-a) in high-latitude regions in winter when there was no light (north of 80° N in December and January, and north of 88° N in November and February). 2) Whenever SIC was greater than 99 %, Chl-a was set to 0.01 mg m^{-3} (full ice coverage, thus minimum Chl-a). We chose the strict criterion of SIC > 99 % because weak but significant primary production has been found to occur under the sea ice in regions with SIC around 90 % (Gosselin et al., 1997; Ulfsbo et al., 2014; Assmy et al., 2017). 3) The remaining grid-cells with missing data were filled, wherever possible, using the average of Chl-a in the surrounding grid-cells within ±1° latitude and ±1° longitude; this mainly compensated for missing Chl-a values due to cloud cover or grid-cells masked out as potentially affected by CDOM and TSM. 4) Parts of the remaining missing Chl-a values, mainly for the pre-satellite period of January–August 1997, were set to the monthly climatological Chl-a values based on the 18-year monthly mean from 1997 to 2014. 5) The final remaining missing Chl-a data, mainly for the marginal sea-ice zone, were generated by linear interpolation using surrounding data. With each interpolation step the number of the grid-cells with missing data decreased; 23 % of grid-cells without Chl-a data were filled by the first step, and the subsequent steps provided data for the remaining 12, 8, 5, and 52 %.

3.3. Gridding of pCO_2 data

In order to bring the individual pCO_{2w} data to the same resolution as the other input data, they were gridded to 1° × 1° × 1 month grid-cells covering the years from 1997 to 2014. This was carried out using the same three-step procedure of Yasunaka et al. (2016) as this excludes values that deviate largely from the long-term mean in the area of each grid cell. In short, first, anomalous values were screened in the following manner. We calculated the long-term mean and its standard deviation for a window size of ±5° of latitude, ±30° of longitude, and ±2 months (regardless of the year) for each 1° × 1° × 1 month grid-cell. We then eliminated the data in each grid-cell that differed by more than three standard deviations from this long-term mean. In the second step, we recalculated the long-term mean and its standard deviation using a smaller window size of ±2° of latitude, ±10° of longitude, and ±1 month (regardless of the year) for each 1° × 1° × 1 month grid-cell, and eliminated data that differed from that long-term mean by more than three standard deviations. In the final step the mean value of the remaining data in each 1° × 1° × 1 month grid cell for each year from 1997 to 2014 was calculated. This procedure identified in total about 0.5 % of the data as extreme values. These may well be correct observations, but likely reflect small spatial scale and/or short time scale

variations that can are quite atypical of the large-scale variability of interest in this study. These excluded values were randomly distributed in time and space.

Although some studies have used pCO_{2w} normalized to a certain year, based on the assumption of a constant rate of increase for pCO_{2w} (e.g., Takahashi et al., 2009), we used "non-normalized" pCO_{2w} values from all years; therefore, in our analysis pCO_{2w} can increase both non-linearly in time and non-uniformly in space.

3.4. pCO_2 estimation using a self-organizing map

We estimated pCO_{2w} by the SOM technique used by Yasunaka et al. (2016), but with Chl-a as an added training parameter to the SOM in addition to SST, SSS, SIC, xCO_{2a}, and geographical position X (=sin[latitude] × cos[longitude]) and Y (=sin[latitude] × sin[longitude]). Chl-a, SST, SSS, and SIC are closely associated with processes causing variation in pCO_{2w}, such as primary production, warming/cooling, mixing, and freshwater input, and represent spatio-temporal pCO_{2w} variability at seasonal to interannual time-scales. Including the xCO_{2a} enables the SOM to reflect the pCO_{2w} time-trend in response to the atmospheric CO_2 changes including large seasonal variation and continued anthropogenic emissions. In several previous studies the anthropogenic pCO_{2w} increase has been assumed to be steady and homogeneous, and

subtracted from the original pCO_{2w} data and added to the estimated pCO_{2w} (Nakaoka et al. 2013; Zheng et al. 2014). However, the occurrence of steady and homogeneous pCO_{2w} trends has not yet been demonstrated in the Arctic Ocean and using xCO_{2a} as a training parameter in the SOM, similar to Landschutzer et al. (2013, 2014) is preferable. Finally, the inclusion of geographical position among the training parameters can prevent systematic spatial biases (Yasunaka et al., 2014). Compared to other efforts mapping pCO_{2w} using the SOM technique such as those by Telszewski et al. (2009) and Nakaoka et al. (2013), we used xCO_{2a}, and geographical position as training parameters while we did not use mixed layer depth because of lack of reliable data in the Arctic.

Briefly, the SOM technique was implemented as follows: first, the approximately one million 1° × 1° × 1 month grid-cells in the analysis region and period were assigned to 5000 groups, which are called "neurons", of the SOM by using the training parameters. Then, each neuron was labeled, whenever possible, with the pCO_{2w} value of the grid-cell where the Chl-a, SST, SSS, SIC, xCO_{2a}, and X and Y values were most similar to those of the neuron. Finally, each grid-cell in the analysis region and period was assigned the pCO_{2w} value of the neuron whose Chl-a, SST, SSS, SIC, xCO_{2a}, and X and Y values were most similar to those of that grid-cell. If the most similar neuron was not labeled with a pCO_{2w} value, then the pCO_{2w} value of the neuron that was most similar

and labeled was used. That case often happened in periods and regions without any observed data. A detailed description of the procedure can be found in Telszewski et al. (2009) and Nakaoka et al. (2013).

3.5. Calculation of air–sea CO_2 fluxes

We calculated monthly air–sea CO_2 flux (F) values from the pCO_{2w} values estimated in Sect. 3.4 by using the bulk formula:

$$F = kL(pCO_{2w} - pCO_{2a}) , \qquad (2)$$

where k is the gas transfer velocity and L is the solubility of CO_2. The solubility of CO_2 (L) was calculated as a function of SST and SSS (Weiss, 1974). We converted the interpolated NOAA marine boundary layer xCO_{2a} data (Sect. 2.2) to pCO_{2a} by using monthly sea-level pressure data and the water-vapor saturation pressure calculated from monthly SST and SSS (Murray, 1967).

The gas transfer velocity k was calculated by using the formula of Sweeney et al. (2007):

$$k = 0.19\ (Sc/660)^{-0.5} <W_{NCEP2}^2>\ , \quad (3)$$

where Sc is the Schmidt number of CO_2 in seawater at a given SST, calculated according to Wanninkhof (2014), "< >" denotes the monthly mean, and $<W_{NCEP2}^2>$ is the monthly mean of the second moment of the NCEP2 6-hourly wind speed. The coefficient 0.19, which is the global average of $0.27<W_{NCEP1}^2>/<W_{NCEP2}^2>$, is based on the one determined by Sweeney et al. (2007) but optimized for NCEP2 winds, following the same method as Schuster et al. (2013) and Wanninkhof et al. (2013).

The suppression of gas exchange by sea ice was accounted for by correcting the air–sea CO_2 fluxes using the parameterization presented by Loose et al. (2009); the flux is proportional to $(1\text{-SIC})^{0.4}$. Following Bates et al. (2006), in the regions with SIC > 99 %, we used SIC = 99 % to allow for non-negligible rates of air–sea CO_2 exchange through leads, fractures, and brine channels (Semiletov et al., 2004; Fransson et al., 2017). This parameterization reduces the flux in fully ice covered waters (SIC > 99%) by 84%.

4. Uncertainty

4.1. Uncertainty in chlorophyll-a concentration data

Fig. 3 shows original and interpolated Chl-a for the year 2012 as an example. Overall,

the interpolated Chl-a data seems to fit well with the original data. Most interpolated Chl-a data have low concentrations because of high SIC and lack of sunlight. The average of the interpolated Chl-a values is 0.1 mg m^{-3}, and less than 5% of the interpolated Chl-a values are >0.5 mg m^{-3} (cf. the average of the original Chl-a values is 1.1 mg m^{-3}, and 48% of the original Chl-a values are >0.5 mg m^{-3}). The previous studies to estimate pCO_{2w} in high-latitudes assumed missing Chl-a as constant values and ignored spatio-temporal variation of Chl-a (Landschutzer et al. 2013; Nakaoka et al. 2013). However, original Chl-a values in the ice-edge region are not small as captured by Perrette et al. (2011), and those in the northernmost grids in winter, north of which the original Chl-a values are missing, is far south of polar night region, since they are missing not because of no sunlight but because of low-angles of sunlight (Fig. 3a). Therefore, we believe interpolation is better than lowest constant values.

To validate our Chl-a interpolation, we repeated the interpolation after randomly eliminating 10 % of the satellite Chl-a values. We then used the eliminated original Chl-a data as independent data for the validation. Note that this comparison was done where there were the original Chl-a data, i.e. the high Chl-a region. The root mean square difference (RMSD) and correlation coefficient between the interpolated and the independent original Chl-a data are 0.90 mg m^{-3} and 0.80, respectively. It means the

interpolated Chl-a, maybe not quantitatively, but qualitatively reproduced the original Chl-a, and therefore is a meaningful parameter in the SOM process. Actually Chl-a data improved the pCO_{2w} estimate, even though Chl-a values in many grid-cells were interpolated values (see Sec. 5.4).

To evaluate our choice of Chl-a algorithm (i.e. the Arctic algorithm of Cota et al., 2004), we compared its calculated Chl-a values with those determined by using the standard algorithm of O'Reilly et al. (1998) and the coastal algorithm of Tassan (1994). RMDS and correlation coefficient (r) between the original (i.e. non-interpolated) Chl-a values are about 0.8 mg m^{-3} and 0.9, respectively (Table 1). For all the Chl-a values including the interpolated data, they are about 0.4 mg m^{-3} and 0.9. The lower RMSD in this case results from the fact that most of the interpolated Chl-a values have low concentrations. This result means the Chl-a from the different algorisms, maybe not quantitatively, but qualitatively consistent with each other. Since not absolute Chl-a values but relative values affect the pCO_{2w} estimates in the SOM technique, the large RMSD among the Chl-a does not result in the significant difference of the pCO_{2w} estimates. Actually, the pCO_{2w} and CO_2 fluxes determined using Chl-a from any of these algorithms as input to the SOM are consistent within their uncertainties (see Sects. 4.2 and 4.3 below). RMSDs between the observed and estimated pCO_{2w} are smallest in

pCO_{2w} estimate using Chl-a from the Arctic algorism, but the differences are quite small (<1%).

4.2. Uncertainty of pCO_{2w} mapping

Fig. 4 compares observed and estimated pCO_{2w} (note that the spatial change visible in Figs. 4a and 4b include differences generated by different seasonal coverage of data in the various regions). Both observed and estimated pCO_{2w} tend to be higher in the subpolar North Atlantic, the Laptev Sea, and the Canada Basin, and lower in the Greenland Sea and the Barents Sea. However, the east–west contrast in the Bering Sea and the contrast between the Canada Basin and the Chukchi Sea are weaker in our estimates than in the observations, and mean bias and RMSD are relatively large in those areas (Figs. 4c and 4d). The temporal changes in the observed and estimated pCO_{2w} are in phase (Fig. 5a), although the variability of the estimated values is somewhat suppressed compared to that of the observed data (Note that the temporal change depicted in Fig. 5a also includes changes incurred by time variations in data coverage). The mean bias and RMSD fluctuate seasonally but are at a constant level over the years (Fig. 5b).

The correlation coefficient between estimated and observed pCO_{2w} is 0.82, and the

RMSD is 30 µatm, which is 9 % of the average and 58 % of the standard deviation of the observed pCO_{2w} values. This is a performance level categorized as "good" by Maréchal (2004). The differences between the estimated and observed values stem not only from the estimation error but also from the error of the gridded observed data. The uncertainty of the pCO_{2w} measurements is 2–5 µatm (Bakker et al., 2014), the uncertainty of the pCO_{2w} values calculated from dissolved inorganic carbon and total alkalinity, whose uncertainties are within 4 µmol kg^{-1} and 6 µmol kg^{-1}, respectively (Olsen et al., 2016), can be up to 14 µatm (Lueker et al., 2000), and the sampling error of the gridded pCO_{2w} observation data was determined from the standard errors of monthly observed pCO_{2w} in the 1° × 1° grid-cells, to 7 µatm (Yasunaka et al., 2016).

To validate our estimated pCO_{2w} values for periods and regions without any observed data, we repeated the mapping experiments after systematically excluding some of the observed pCO_{2w} data when labeling the neurons; four experiments were carried out, by excluding data (1) from 1997–2004, (2) from January to April, (3) from north of 80°N, and (4) from the Laptev Sea (90°E – 150°E), where there are only a few pCO_{2w} observations. We compared the pCO_{2w} estimates obtained in each experiment with the excluded observations and found that the pCO_{2w} estimates reproduced the general features of the excluded data, both spatially and temporally (not shown here). They

were also similar to the pCO_{2w} estimates obtained by using all observations, although the RMSDs between the estimates and the excluded observations are 54 μatm on average, which is 1.8 times the RMSDs of the estimates based on all observations. It means that our estimated pCO_{2w} reproduce the general features both in space and time even when and where there are no observed data, although the uncertainty in pCO_{2w} might be as large as 54 μatm in regions and periods without data. We used this uncertainty for pCO_{2w} estimates made by using the pCO_{2w} values of a less similar neuron.

4.3. Uncertainty of CO_2 flux estimates

Signorini and McClain (2009) estimated the uncertainty of the CO_2 flux resulting from uncertainties in the gas exchange parameterization to be 36 %, and that resulting from uncertainties in the wind data to be 11 %. The uncertainty for SIC is 5 % (Cavalieri et al., 1984; Gloersen et al., 1993; Peng et al., 2013). The standard error of the sea-ice effect on gas exchange was estimated to about 30 % by Loose et al. (2009). The uncertainty of pCO_{2a} is about 0.5 μatm (http://www.esrl.noaa.gov/gmd/ccgg/mbl/mbl.html), and that of pCO_{2w} was 30 μatm (Sect. 4.2); therefore, we estimated the uncertainty of ΔpCO_2 ($=pCO_{2w} - pCO_{2a}$) to be

34 % (average ΔpCO_2 in the analysis domain and period was −89 µatm). The overall uncertainty of the estimated CO_2 fluxes is thus 59 % ($[0.36^2 + 0.11^2 + 0.05^2 + 0.3^2 + 0.34^2]^{1/2}$) in sea-ice covered regions and 51 % ($[0.36^2 + 0.11^2 + 0.34^2]^{1/2}$) in ice-free regions. For estimates using the pCO_{2w} values of a less similar neuron, whose uncertainty in pCO_{2w} is 54 µatm and the uncertainty of the ΔpCO_2 estimates can be as high as 61 %, the uncertainty is 78 % ($[0.36^2 + 0.11^2 + 0.05^2 + 0.3^2 + 0.61^2]^{1/2}$) in sea-ice covered regions, and 72 % ($[0.36^2 + 0.11^2 + 0.61^2]^{1/2}$) in ice-free regions. The average of the estimated CO_2 flux in the analysis domain and period is 4.8 mmol m^{-2} d^{-1}; hence the uncertainty of the CO_2 flux estimate corresponds to 2.8 mmol m^{-2} d^{-1} in sea-ice covered regions and 2.4 mmol m^{-2} d^{-1} in ice-free regions. For estimates using the pCO_{2w} values of a less similar neuron, the uncertainty corresponds to 3.7 mmol m^{-2} d^{-1} in the sea-ice covered region and 3.5 mmol m^{-2} d^{-1} in ice-free regions.

5. Results and discussion

5.1. Relationship between pCO_2 and chlorophyll-a

Fig. 6 compares the observed pCO_{2w} and the original non-interpolated Chl-a in spring (March–May) and summer (July–September). In spring, when much of the Arctic Ocean is ice-covered, Chl-a is high in the Barents Sea and the Bering Strait (>1 mg m^{-3}). In

summer, when the ice cover is less extensive, Chl-a is high in the Chukchi Sea, the Kara Sea, the Laptev Sea, and the East Siberian Sea (>1 mg m^{-3}) and especially high in the coastal regions of the two latter (>2 mg m^{-3}). pCO_{2w} is high in the Norwegian Sea in spring, and in the Kara Sea, the Laptev Sea and the Canada Basin during summer (>300 μatm). On the other hand, it is lower in the Chukchi Sea, Bering Strait area and the sea-ice edge region of the Eurasian Basin in summer (<300 μatm). The overall correlation between pCO_{2w} and Chl-a is negative where Chl-a ≤ 1 mg m^{-3} (70% of all the data; correlation coefficient $r = -0.36$, $P < 0.01$), but there is no significant relationship where Chl-a > 1 mg m^{-3} (Fig. 7). A similar situation was identified in the subpolar North Atlantic by Olsen et al. (2008). It means that primary production generally draws down the pCO_{2w}, but high Chl-a are not necessarily associated with the low pCO_{2w} probably because high Chl-a usually appears in the coastal regions (Fig. 6b; see below).

To determine the spatial variability of the relationship between pCO_{2w} and Chl-a, we calculated the correlation coefficients between pCO_{2w} and Chl-a in a window of ±5° of latitude, and ±30° of longitude for each monthly 1° × 1° grid-cell (Fig. 8a). The correlations between pCO_{2w} and Chl-a are negative in the Greenland/Norwegian Seas and over the Canada Basin. In the Greenland/Norwegian Seas, the correlation between

pCO_{2w} and Chl-a is strongly negative ($r < -0.4$) in spring and weakly negative ($-0.4 < r < 0$) in summer. Chl-a there is higher in summer than in spring (Fig. 6b), whereas nutrient concentrations are high in spring and low in summer (Fig. 8b). Taken together, this suggest that primary production draws down the pCO_{2w} in spring, whereas in summer the primary production mostly depends on regenerated nutrients (Harrison and Cota, 1991) and the net CO_2 consumption is small, as also reported for the subpolar North Atlantic (Olsen et al., 2008). Therefore the correlation between pCO_{2w} and Chl-a becomes less negative. In the eastern Barents Sea, the Kara Sea and the East Siberian Sea, and the Bering Strait, the correlations are positive because of water with high pCO_{2w} and Chl-a in the coastal region subjected to river discharge (Murata, 2006; Semiletov et al., 2007; Anderson et al., 2009; Manizza et al., 2011). In the Chukchi Sea, the relationship is weak ($-0.2 < r < 0.2$), probably because the relationship is on smaller spatial and temporal scales than those represented by the window size used here, as shown by Mucci et al. (2010). The occurrence of calcifying plankton blooms in this region, likely also weakens the correlation since the calcification increases pCO_{2w} (Shutler et al., 2013; Fransson et al., 2017).

These results show that pCO_{2w} relates Chl-a, but the relationships are different depending on the region and the season. It is difficult to represent such a complex

relationship using simple equations (e.g. multiple regression methods) because it needs a priori assumptions of regression functions and of dividing the basin into sub-regions. But the SOM technique can empirically induce the relationships without any of the a priori assumptions, and therefore is suitable to represent such a complex relationship.

5.2. Spatiotemporal CO_2 flux variability

The 18-year annual mean CO_2 flux distribution shows that all areas of the Arctic Ocean and its adjacent seas were net CO_2 sinks over the time period that we investigated (Fig. 9). The annual CO_2 influx to the ocean was strong in the Greenland/Norwegian Seas (9 ± 3 mmol m^{-2} d^{-1}; 18-year annual mean ± uncertainty averaged over the area shown in Fig. 1), the Barents Sea (10 ± 3 mmol m^{-2} d^{-1}), and the Chukchi Sea (5 ± 3 mmol m^{-2} d^{-1}). In contrast, influx was weak and not statistically significantly different from zero in the Eurasian Basin, the Canada Basin, the Laptev Sea and the East Siberian Sea. Our annual CO_2 flux estimates are consistent with those reported by Yasunaka et al. (2016) and other previous studies (Bates and Mathis, 2009, and references therein).

The estimated 18-year average CO_2 influx to the Arctic Ocean was 5 ± 3 mmol m^{-2} d^{-1}, equivalent to an uptake of 180 ± 130 TgC y^{-1} for the ocean area north of 65° N,

excluding the Greenland/Norwegian Seas and Baffin Bay (10.7×10^6 km^2; see Fig. 1). This accounts for 12% of the net global CO_2 uptake by the ocean of 1.5 Gt C yr^{-1} (Gruber et al., 2009; Wanninkhof et al., 2013; Landschützer et al., 2014). It is within the range of other estimates (81–199 TgC y^{-1}; Bates and Mathis, 2009), but close to the upper bound. That is partly because the parameterization of the suppression effect by sea ice used in this study. Using another parameterization which represents the SIC effect linearly (Takahashi et al. 2009; Butterworth and Miller 2016), CO_2 uptake of the Arctic Ocean was estimated to be 130 ± 110 TgC y^{-1}.

Fig. 10 shows the seasonal variation of the air-sea CO_2 fluxes and its controlling factors (ΔpCO_2, wind speed and SIC; solubility is not shown as the impacts of its variations are relatively small in this context) in the Greenland/Norwegian Seas, the Barents Sea, the Chukchi Sea and the Arctic Ocean. In all of these regions the influxes are strongest in October, when the winds strengthen with the approach of winter and the pCO_{2w} and/or SIC are still as low as in the summer. In the Greenland/Norwegian Seas and the Barents Sea the CO_2 influx shows a secondary maximum in February because the strongest winds occur in that month, while in the Chukchi Sea and Arctic Ocean, the winds are also strong but the flux is suppressed by the extensive sea-ice cover. All of these regions are undersaturated with pCO_{2w} (i.e. negative ΔpCO_2) throughout all

seasons. The undersaturation is strongest in the Arctic Ocean, as this has the most extensive sea ice cover limiting the fluxes from the atmosphere and the strongest stratification, limiting the mixing of CO_2 rich subsurface waters into the surface ocean. The undersaturation typically shows a maximum (i.e. ΔpCO_2 is minimum) in late spring to early summer (May–June) when the spring bloom occur (Pabi et al. 2008), but not in the Arctic Ocean. Here the undersaturation reaches its minimum (ΔpCO_2 is the smallest) in late summer (August–September) at the time of minimum sea ice cover, since the seasonal decrease of pCO_2 in summer is larger in the air than in the sea. Overall, in the Greenland/Norwegian Seas and the Barents Sea the seasonal variations of the CO_2 flux is opposite to that expected from the seasonal ΔpCO_2 variations because it is the wind speed that governs most of the seasonal flux variations. In the Chukchi Sea, on the other hand, the CO_2 influx is strongest in summer, a consequence of the minimum sea-ice cover and strongest pCO_2 undersaturation. In the Arctic Ocean it is the SIC and wind speed that drive the seasonal flux variations. Seasonal variations of CO_2 flux are consistent with those of the previous studies (Yasunaka et al. 2016, and references therein), whereas those of pCO_{2w} become realistic (see Section 5.3 below).

Fig. 11 shows interannual variation of CO_2 flux and its driving factors in these four regions. The interannual variations of CO_2 flux and ΔpCO_2 are generally smaller than

the seasonal variations, and are often smaller than their respective uncertainty. In the Greenland/Norwegian Sea, interannual variation of the CO_2 flux negatively correlates with the wind speed (CO_2 influx to the ocean is large when the wind is strong; r = –0.41), while interannual variation of ΔpCO_2 and sea ice change is small. In the Barents Sea, the interannual variation of CO_2 flux correlates with ΔpCO_2 positively (r = 0.71) and with SIC negatively (r = –0.50), while the correlation with wind speed is not significant. Although low SIC enhance the air-sea CO_2 exchange due to increase of the area of open water, it also associates with high SST and therefore high pCO_{2w} there. In the Chukchi Sea, CO_2 influx to ocean is decreasing with the increasing of ΔpCO_2 (r = 0.87). High pCO_{2w} (>500 μatm) via storm-induced deep mixing events has been sometimes observed in the Chukchi Sea after 2010 (Hauri et al. 2013; Taro Takahashi, personal communication). Interannual variability of the CO_2 flux averaged over the Arctic Ocean is small because the increasing ΔpCO_2 is compensated by the effect of sea ice retreat (r = –0.70). Thus, the combined effect of sea-ice retreat and pCO_{2w} increase on CO_2 flux varied among regions.

The CO_2 influx has been increasing in the Greenland Sea and northern Barents Sea, and decreasing in the Chukchi Sea and southern Barents Sea (Fig. 12). The CO_2 flux trend corresponds well with the ΔpCO_2 trend, which in turn corresponds well with the

SST trend. The increasing CO_2 influx in the northern Barents Sea also corresponds with the sea-ice retreat. These results are similar to that for the previous estimates without using Chl-a (see Fig. 10 in Yasunaka et al., 2016). It shows again that the combined effect of sea-ice retreat and pCO_{2w} increase to the CO_2 flux is regionally different. In the SOM process, the pCO_{2w} values observed in the latter period might be used for the pCO_{2w} estimate in the former period where the pCO_{2w} measurements have not been made, and therefore the trend in CO_2 influx might be affected by the spatio-temporal distribution of the measurements. To confirm this is not the case, we checked that the spatial distribution of the pCO_{2w} trend did not correspond to the year when the first observation was conducted (see supplement).

5.3. Impact of incorporating chlorophyll-a data in the SOM

To determine the impact of including Chl-a data in the SOM process, the analyses were repeated without Chl-a data. The RMSD of the resulting estimated pCO_{2w} values is 33 μatm, which is 3 μatm larger than the uncertainty of the estimates generated by including Chl-a in the SOM. Chl-a data thus improved the pCO_{2w} estimate (namely, a 10 % reduction of RMSD), even though 40 % of the Chl-a data labeled with pCO_{2w} observations were interpolated Chl-a values.

Figs. S1 and S2 present the difference in bias and RMSD for pCO_{2w} estimated with and without Chl-a; Fig. S1 shows the time-evolution and Fig. S2 shows the spatial distribution. Both approaches typically underestimate pCO_{2w} in winter and overestimate the summertime values, but these systematic biases are reduced when Chl-a are included in the SOM (Fig. S1). Biases and RMSDs are reduced in the Canada basin, the western Bering Sea, and the boundary region between the Norwegian Sea and the subpolar North Atlantic (Fig. S2). As a result the strong east–west contrast in the Bering Sea and the contrast between the Canada Basin and the Chukchi Sea (see Fig. 4) are better represented when Chl-a is included. Taken together, inclusion of Chl-a when estimating pCO_{2w} yields not only better representation of the pCO_{2w} decline in spring and summer but also improves the representation of the spatio-temporal pCO_{2w} distribution. Technically, these improvements come from the fact that Chl-a as a training parameter can separate high Chl-a region/time and low Chl-a region/time into different neurons, which contaminated in the same neurons trained without Chl-a. For example, since Chl-a is high in spring but SST and SIC are still in the similar levels with winter, the grid-cells in spring and winter would be classified into the separate neurons when Chl-a is included as a training parameter, but in the same neuron when Chl-a is not included. As a result, without Chl-a, the estimated pCO_{2w} in spring tends to be similar to

the pCO_{2w} in winter, and the pCO_{2w} in winter tends to be similar to that in spring. And therefore the contrast between winter and spring is weakened without Chl-a.

The seasonal cycles of pCO_{2w} estimates derived with the inclusion of Chl-a have a larger amplitude than the uncertainties, whereas the uncertainties are larger than the seasonal amplitude when pCO_{2w} is derived without Chl-a (upper panels of Fig. 13). The difference is caused by the fact that the seasonal cycle of pCO_{2w} in each region reproduces the observed cycle better when Chl-a was included (lower panels of Fig. 13). Note that the much larger seasonal amplitude in the lower panels is an artefact generated by the seasonal bias in sampling locations; in winter most measurements are obtained at low latitudes where pCO_{2w} is typically higher than at high latitudes.

Compared to the CO_2 influx estimates by Yasunaka et al. (2016), the winter CO_2 influx in the Greenland/Norwegian Seas estimated including Chl-a is about 3 mmol m^{-2} d^{-1} less than that calculated without using Chl-a (Fig. 14), but this difference is smaller than the uncertainties. The CO_2 fluxes in the other area are quite similar with each estimate, while their uncertainties are smaller in the present estimates.

The inclusion of Chl-a data also reduced the uncertainty of the estimated annual air-sea CO_2 flux integrated over the entire Arctic Ocean. Compared to the flux estimate determined by Yasunaka et al. (2016) of 180 ± 210 TgC y^{-1}, the CO_2 uptake in the

Arctic Ocean estimated here is significant within its uncertainty (180 ± 130 TgC y^{-1}). This improvement is the result of 1) the inclusion of Chl-a data in the SOM process (which reduced the uncertainty by 23 %); 2) the separate uncertainty estimates for ice-free and ice-covered regions (8 %); and 3) the addition of new observational pCO_{2w} data (7 %). Reducing the uncertainty of this quantification is a key contribution to the larger work of constraining the global carbon budget (e.g., Le Quere et al., 2016). Because the Arctic is an important CO_2 sink, quantifying its fluxes and minimizing the uncertainty is of great scientific value.

5.4. Toward further reduction of the uncertainty

The addition of new observational data from SOCATv4 and GLODAPv2 reduced the overall uncertainty in the mapped pCO_{2w}: a 33 % increase in the number of observations induced a 7 % reduction in the uncertainty. However, there are still few observations in the Kara Sea, the Laptev Sea, the East Siberian Sea and the Eurasian Basin (Fig. 2). To improve our understanding of the variability in air–sea CO_2 fluxes in the Arctic, it is of critical importance to obtain additional ocean CO_2 measurements to fill these data gaps, and that these measurements are made publically available. Data synthesis activities like SOCAT must be encouraged.

In the present study, we discussed the combined effect of sea-ice retreat and pCO_{2w} change on the air-sea CO_2 flux. There are other factors that will induce the change of CO_2 flux. For example, warmer temperature will lead to an increasing buffering capacity while lower salinity will have the opposite effect and cause a decrease in buffering capacity. In our current study, we used climatological-mean salinity for the pCO_{2w} estimate because of lack of reliable year-to-year salinity data. That might be one of the improvements for a future study.

6. Conclusions

By applying an SOM technique with the inclusion of Chl-a data to estimate pCO_{2w}, we produced monthly maps of air–sea CO_2 fluxes from 1997 to 2014 for the Arctic Ocean and its adjacent seas north of 60° N. Negative correlation between pCO_{2w} and Chl-a meant that Chl-a is valuable parameter to represent primary production. Since the relationship varied among seasons and regions, the SOM technique is better suited for the mapping than a multiple linear regression approach. Adding Chl-a to the SOM process improved representation of the seasonal cycle of pCO_{2w}, and therefore reduced the uncertainty of the CO_2 flux estimates.

In the Greenland/Norwegian Seas and the Barents Sea the CO_2 influx was large in

autumn and winter because of the strong wind. In the Chukchi Sea, on the other hand, the CO_2 influx was strong in summer and autumn, as a consequence of the low SIC and strong pCO_{2w} undersaturation. Although interannual variation of the CO_2 influx was smaller than the seasonal variation, the CO_2 influx has been increasing in the Greenland Sea and northern Barents Sea, and decreasing in the Chukchi Sea and southern Barents Sea.

A major goal of the carbon-cycle research community in recent years has been to reduce the uncertainty in estimates of carbon reservoirs and fluxes. Our results contribute to this in that CO_2 uptake in the Arctic Ocean is demonstrated with high significance. The resulting estimate of the annual Arctic Ocean CO_2 uptake of 180 TgC y^{-1} is significant with an uncertainty of ± 130 TgC y^{-1}. This is a substantial improvement over earlier estimates, and is due mainly to the incorporation of Chl-a data.

Assessment of the numerical models using our estimate of Arctic carbon uptake is also an interesting topic since numerical models are poorly validated in the Arctic due to the limited observations of biogeochemistry (Popova et al., 2012). However, such experiments need thorough insight into the numerical models, which is beyond the scope of this study. We hope to perform such comparisons in future studies.

The monthly CO_2 flux, pCO_{2w}, and interpolated Chl-a data presented in this paper will be available at the JAMSTEC website (http://www.jamstec.go.jp/res/ress/yasunaka/co2flux_v2).

Acknowledgments

We thank the many researchers and funding agencies responsible for the collection of data and quality control for their contributions to SOCAT and GLODAPv2. We are grateful for the use of the CO2SYS program obtained from the Ocean Carbon Data System of NOAA National Centers for Environmental Information (https://www.nodc.noaa.gov/ocads/oceans/CO2SYS/co2rprt.html), and SOM Toolbox Version 2 developed by the Laboratory of Information and Computer Science at Helsinki University of Technology (http://www.cis.hut.fi/projects/somtoolbox). We thank ACRI-ST, France, for developing, validating, and distributing the GlobColour data used in this work. This work was financially supported by the Arctic Challenge for Sustainability (ArCS) Project funded by the Ministry of Education, Culture, Sports, Science and Technology, Japan. Are Olsen was supported by grants from the Norwegian Research Council (Subpolar North Atlantic Climate States [SNACS] 229752 and the Norwegian component of the Integrated Carbon Observation System [ICOS-Norway]

245927). Mario Hoppema was partly supported by the German Federal Ministry of Education and Research (grant no. 01LK1224I; ICOS-D). Siv K. Lauvset acknowledges support from the Norwegian Research Council (VENTILATE, 229791) and the EU H2020 project AtlantOS (grant agreement no. 633211). Rik Wanninkhof and Taro Takahashi acknowledge support from the Office of Oceanic and Atmospheric Research (OAR) of the United States NOAA, including resources from the Ocean Observation and Monitoring Division of the Climate Program Office (fund reference100007298).

References

Anderson, L. G., Jutterström, S., Hjalmarsson, S., Wåhlström, I., and Semiletov, I. P.: Out-gassing of CO_2 from Siberian Shelf seas by terrestrial organic matter decomposition, Geophys. Res. Lett., 36, L20601, doi:10.1029/2009GL040046, 2009.

Ardyna, M., Babin, M., Gosselin, M., Devred, E., Rainville, L., and Tremblay, J.-É.: Recent Arctic Ocean sea ice loss triggers novel fall phytoplankton blooms, Geophys. Res. Lett., 41, 6207–6212, doi:10.1002/2014GL061047, 2014.

Arrigo, K. R., and van Dijken, G. L.: Annual cycles of sea ice and phytoplankton near Cape Bathurst, southeastern Beaufort Sea, Canadian Arctic, Geophys. Res. Lett., 31, L08304, doi:10.1029/2003GL018978, 2004.

Assmy P. M. Fernandez-Mendez, Duarte, P., Meyer, A., Randelhoff, A., Mundy, C. J., Olsen, L. M., Kauko, H. M., Bailey, A., Chierici, M., Cohen, L., Doulgeris, A. P., Ehn, J. K., Fransson, A., Gerland, S., Hop, H., Hudson, S. R., Hughes, N., Itkin, P. , Johnsen, G. , King, J. A., Koch, B. P. , Koenig, Z., Kwasniewski, S., Laney, S. R., Nicolaus, M., Pavlov, A. K., Polashenski, C. M., Provost, C., Rösel, A., Sandbu, M., Spreen, G., Smedsrud, L. H., Sundfjord, A., Taskjelle, T., Tatarek, A., Wiktor, J., Wagner, P. M., Wold, A., Steen, H., and Granskog, M. A.: Leads in Arctic pack ice enable early phytoplankton blooms below snow-covered sea ice. Scientific Report, 7:40850, DOI: 10.1038/srep40850, 2017.

Bakker, D. C. E., Pfeil, B., Smith, K., Hankin, Olsen, A., Alin, C. Cosca, S. R., Harasawa, S., Kozyr, A., Nojiri, Y., O'Brien, K. M., Schuster, U., Telszewski, M., Tilbrook, B., Wada, C., Akl, J., Barbero, L., Bates, N., Boutin, J., Cai, W.-J., Castle, R. D., Chavez, F. P., Chen, L., Chierici, M., Currie, K., de Baar, H. J. W., Evans, W., Feely, R. A., Fransson, A., Gao, Z., Hales, B., Hardman-Mountford, N., Hoppema, M., Huang, W.-J., Hunt, C. W., Huss, B., Ichikawa, T., Johannessen, T., Jones, E. M., Jones, S., Jutterstrøm, S., Kitidis, V., Körtzinger, A., Lauvset, S. K., Lefèvre, N., Manke, A. B., Mathis, J. T., Merlivat, L., Metzl, N., Murata, A., Newberger, T., Ono, T., Park, G.-H., Paterson, K., Pierrot, D., Ríos, A. F., Sabine, C. L., Saito, S.,

Salisbury, J., Sarma, V. V. S. S., Schlitzer, R., Sieger, R., Skjelvan, I., Steinhoff, T., Sullivan, K., Sun, H., Sutton, A. J., Suzuki, T., Sweeney, C., Takahashi, T., Tjiputra, J., Tsurushima, N., van Heuven, S. M. A. C., Vandemark, D., Vlahos, P., Wallace, D. W. R., Wanninkhof, R., and Watson, A. J.: An update to the Surface Ocean CO_2 atlas (SOCAT version 2). Earth System Science Data, 6, 69–90, doi:10.5194/essd-6-69-2014, 2014.

Bakker, D. C. E., Pfeil, B., Smith, K., Harasawa, S., Landa, C., Nakaoka, S., Nojiri, Y., Metzl, N., O'Brien, K. M., Olsen, A., Schuster, U., Tilbrook, B., Wanninkhof, R., Alin, S. R., Barbero, L., Bates, N. R., Bianchi, A. A., Bonou, F., Boutin, J., Bozec, Y., Burger, E., Cai, W.-J., Castle, R. D., Chen, L., Chierici, M., Cosca, C., Currie, K., Evans, W., Featherstone, C., Feely, R. A., Fransson, A., Greenwood, N., Gregor, L., Hankin, S., Hardman-Mountford, N. J., Harlay, J., Hauck, J., Hoppema, M., Humpt, L., Monteiro, P., Munro, D., Murata, A., Newberger, T., Omar, A. M., Ono, T., Paterson, K., Pierrot, D., Robbins, L. L., Sabine, C. L., Saito, S., Salisbury, J., Schneider, B., Schlitzer, R., Sieger, R., Skjelvan, I., Steinhoff, T., Sullivan, K. F., St, L., Monteiro, P., Munro, D., Murata, A., Newberger, T., Omar, A. M., Ono, T., Paterson, K., Pierrot, D., Robbins, L. L., Sabine, C. L., Saito, S., Salisbury, J., Schneider, B., Schlitzer, R., Sieger, R., Skjelvan, I., Steinhoff, T., Sullivan, K. F.,

Sutherland, S. C., Sutton, A. J., Sweeney, C., Tadokoro, K., Takahashi, T., Telszewski, M., Van Heuven, S. M. A. C., Vandemark, D., Wada, C., Ward, B., and Watson, A. J.: A multi-decade record of high quality fCO_2 data in version 3 of the Surface Ocean CO_2 Atlas (SOCAT). Earth System Science Data, 8, 383–413. doi:10.5194/essd-8-383-2016, 2016.

Bates, N. R., and Mathis, J. T.: The Arctic Ocean marine carbon cycle: evaluation of air-sea CO_2 exchanges, ocean acidification impacts and potential feedbacks, Biogeosciences, 6, 2433-2459, doi:10.5194/bg-6-2433-2009, 2009.

Bates, N. R., Moran, S. B., Hansell, D. A., and Mathis, J. T.: An increasing CO_2 sink in the Arctic Ocean due to sea-ice loss, Geophys. Res. Lett., 33, L23609, doi:10.1029/2006GL027028, 2006.

Bates, N. R., Garley, R., Frey, K. E., Shake, K. L., and Mathis J. T.: Sea-ice melt CO_2-carbonate chemistry in the western Arctic Ocean: meltwater contributions to air-sea CO_2 gas exchange, mixed layer properties and rates of net community production under sea ice. Biogeosciences, 11, 6769–6789, doi:10.5194/bg-11-6769-2014., 2014

Boyer, T. P., Antonov, J. I., Baranova, O. K., Coleman, C., Garcia, H. E., Grodsky, A., Johnson, D. R., Locarnini, R. A., Mishonov, A. V., O'Brien, T. D., Paver, C. R.,

Reagan, J. R., Seidov, D., Smolyar, I. V., and Zweng, M. M.: World Ocean Database 2013. Sydney Levitus, Ed.; Alexey Mishonov, Technical Ed.; NOAA Atlas NESDIS 72, 209 pp, 2013.

Butterworth, B. J., and Miller, S. D.: Air-sea exchange of carbon dioxide in the Southern Ocean and Antarctic marginal ice zone. Geophys. Res. Lett., 43, 7223–7230, doi:10.1002/2016GL069581, 2016.

Cai, W.J., Chen, L. Q., Chen, B. S., Gao, Z. Y., Lee, S. H., Chen, J. F., Pierrot, D., Sullivan, K., Wang, Y.C., Hu, X. P., Huang, W. J., Zhang, Y. H., Xu, S. Q., Murata, A., Grebmeier, J. M., Jones, E. P., and Zhang, H. S.: Decrease in the CO_2 uptake capacity in an ice-free Arctic Ocean Basin. Science, 329, 556–559, doi:10.1126/science.1189338, 2010.

Cavalieri, D. J., Gloersen, P., and Campbell, W. J.: Determination of sea ice parameters with the NIMBUS-7 SMMR, J. Geophys. Res., 89, 5355–5369, 1984.

Chierici, M., Olsen, A., Johannessen, T., Trinañes, J., Wanninkhof, R.: Algorithms to estimate CO_2 in the northern North Atlantic using observations, satellite and ocean analysis data, Deep-Sea Res. II, 56, 630–639, doi:10.1016/j.dsr2.2008.12.01, 2009.

Chierici, M, Fransson, A., Lansard, B., Miller, L. A., Mucci, A., Shadwick, E., Thomas, H., Tremblay, J.-E., and Papakyriakou, T.: The impact of biogeochemical processes

and environmental factors on the calcium carbonate saturation state in the Circumpolar Flaw Lead in the Amundsen Gulf, Arctic Ocean. J. Geophys. Res., 116, C00G09, doi:10.1029/2011JC007184, 2011.

Conway, T.J., Tans, P. P., Waterman, L. S., Thoning, K. W., Kitzis, D. R., Masarie, K. A., and Zhang, N.: Evidence for interannual variability of the carbon cycle from the NOAA/CMDL global air sampling network. J. Geophys. Res., 99, 22831–22855, 1994.

Cota, G. F., Wang, J., and Comiso, J. C.: Transformation of global satellite chlorophyll retrievals with a regionally tuned algorithm, Remote Sens. Environ. 89, 326–350, doi:10.1016/j.rse.2004.01.005, 2004.

Dickson, A. G.: Standard potential of the reaction: AgCl(s) + 1/2H_2(g) = Ag(s) + HCl(aq), and the standard acidity constant of the ion HSO_4^- in synthetic seawater from 273.15 to 318.15 K. J. Chemical Thermodynamics, 22, 113–127, 1990.

Else, B. G. T., Galley, R. J., Lansard, B., Barber, D. G., Brown, K., Miller, L. A., Mucci, A., Papakyriakou, T. N., Tremblay, J.-É., and Rysgaard, S.: Further observations of a decreasing atmospheric CO_2 uptake capacity in the Canada Basin (Arctic Ocean) due to sea ice loss, Geophys. Res. Lett., 40, 1132–1137, doi:10.1002/grl.50268, 2013.

Fransson, A., Chierici, M., Skjelvan, I., Olsen, A., Assmy, P., Peterson, A. K., Spreen, G.,

and Ward, B.: Effects of sea-ice and biogeochemical processes and storms on under-ice water fCO_2 during the winter-spring transition in the high Arctic Ocean: Implications for sea-air CO_2 fluxes. J. Geophys. Res., doi:10.1002/2016JC012478, 2017.

Gao, Z., Chen, L., Sun, H., Chen, B., and Cai, W.-J.: Distributions and air–sea fluxes of carbon dioxide in the Western Arctic Ocean, Deep-Sea Res. II, 81–84, 46–52, doi:10.1016/j.dsr2.2012.08.021, 2012.

Gloersen, P., Campbell, W. J., Cavalieri, D. J., Comiso, J. C., Parkinson, C. L., and Zwally, H. J.: Arctic and Antarctic sea ice, 1978–1987: Satellite passive-microwave observations and analysis, NASA Spec. Publ., 511, 290 pp, 1993.

Gosselin, M., Levasseur, M., Wheeler, P. A., Horner, R. A., and B. C. Booth: New measurements of phytoplankton and ice algal production in the Arctic Ocean, Deep-Sea Res. II, 44, 1623–1644, doi:10.1016/S0967-0645(97)00054-4, 1997.

Harrison, W. G., and Cota., G. F.: Primary production in polar waters: relation to nutrient availability, Polar Research, 10, 87–104, doi:10.1111/j.1751-8369.1991.tb00637.x, 1991.

Hauri, C., Winsor, P., Juranek, L. W., McDonell, A. M. P., Takahashi, T. and Mathis, J. T.: Wind-driven mixing causes a reduction in the strength of the continental shelf

carbon pump in the Chukchi Sea, Geophys. Res. Letters, 40, 5932-5936, doi:10.1002/2013GL058267, 2013.

Iida, T., Saitoh, S. I., Miyamura, T., Toratani, M., Fukushima, H., and Shiga, N.: Temporal and spatial variability of coccolithophore blooms in the eastern Bering Sea, 1998-2001, Prog. Oceanogr., 55, 165–175, 2002.

Kalnay, E., Kanamitsu, M., Kistler, R., Collins, W., Deaven, D., Gandin, L., Iredell, M., Saha, S., White, G., Woollen, J., Zhu, Y., Chelliah, M., Ebisuzaki, W., Higgins, W., Janowiak, J., Mo, K. C., Ropelewski, C., Wang, J., Leetmaa, A., Reynolds, R., Jenne, R., and Joseph, D., The NCEP/NCAR 40-Year Reanalysis Project". Bull. Amer. Meteor. Soc., 77, 437–471, 1996.

Kanamitsu, M., Ebisuzaki, W., Woollen, J., Yang, S-K, Hnilo, J. J., Fiorino, M., and Potter, G. L., NCEP-DOE AMIP-II Reanalysis (R-2), Bull. Amer. Meteor. Soc., 83, 1631–1643, 2002.

Key, R.M., Olsen, A., van Heuven, S., Lauvset, S. K., Velo, A., Lin, X., Schirnick, C., Kozyr, A., Tanhua, T., Hoppema, M., Jutterström, S., Steinfeldt, R., Jeansson, E., Ishii, M., Perez, F. F., and T. Suzuki: Global Ocean Data Analysis Project, Version 2 (GLODAPv2), ORNL/CDIAC-162, ND-P093. Carbon Dioxide Information Analysis Center, Oak Ridge National Laboratory, US Department of Energy, Oak Ridge,

Tennessee. doi: 10.3334/CDIAC/OTG.NDP093_GLODAPv2, 2015.

Le Quéré, C., Andrew, R. M., Canadell, J. G., Sitch, S., Korsbakken, J. I., Peters, G. P., Manning, A. C., Boden, T. A., Tans, P. P., Houghton, R. A., Keeling, R. F., Alin, S., Andrews, O. D., Anthoni, P., Barbero, L., Bopp, L., Chevallier, F., Chini, L. P., Ciais, P., Currie, K., Delire, C., Doney, S. C., Friedlingstein, P., Gkritzalis, T., Harris, I., Hauck, J., Haverd, V., Hoppema, M., Klein Goldewijk, K., Jain, A. K., Kato, E., Körtzinger, A., Landschützer, P., Lefèvre, N., Lenton, A., Lienert, S., Lombardozzi, D., Melton, J. R., Metzl, N., Millero, F., Monteiro, P. M. S., Munro, D. R., Nabel, J. E. M. S., Nakaoka, S.-I., O'Brien, K., Olsen, A., Omar, A. M., Ono, T., Pierrot, D., Poulter, B., Rödenbeck, C., Salisbury, J., Schuster, U., Schwinger, J., Séférian, R., Skjelvan, I., Stocker, B. D., Sutton, A. J., Takahashi, T., Tian, H., Tilbrook, B., van der Laan-Luijkx, I. T., van der Werf, G. R., Viovy, N., Walker, A. P., Wiltshire, A. J., and Zaehle, S.: Global Carbon Budget 2016, Earth Syst. Sci. Data, 8, 605-649, https://doi.org/10.5194/essd-8-605-2016, 2016.

Landschützer, P., Gruber, N., Bakker, D. C. E., Schuster, U., Nakaoka, *S.*, Payne, M. R., Sasse, T., *and* Zeng J., A neural network-based estimate of the seasonal to inter-annual variability of the Atlantic Ocean carbon sink, Biogeosciences, 10, 7793–7815, *doi:10.5194/bg-10-7793-2013, 2013.*

Landschützer, P., Gruber, N., Bakker, D. C. E., and Schuster, U.: Recent variability of the global ocean carbon sink, Global Biogeochemical Cycles, 28, 927-949, doi:10.1002/2014GB004853, 2014.

Lefèvre, N., Watson, A. J., and Watson, A. R.: A comparison of multiple regression and neural network techniques for mapping in situ pCO_2 data, Tellus B, 57: 375–384. doi:10.1111/j.1600-0889.2005.00164.x, 2005.

Lewis, E., and Wallace, D. W. R.: Program Developed for CO_2 System Calculations. ORNL/CDIAC-105. Carbon Dioxide Information Analysis Center, Oak Ridge National Laboratory, U.S. Department of Energy, Oak Ridge, Tennessee, 1998.

Lewis, K.M., Mitchell, B.G., van Dijken, G.L., and Arrigo, K.R.: Regional chlorophyll a algorithms in the Arctic Ocean and their effect on satellite-derived primary production estimates, Deep-Sea Res. II, 130, 17–24, doi:10.1016/j.dsr2.2016.04.020, 2016.

Loose, B., McGillis, W. R., Schlosser, P., Perovich, D., and Takahashi, T.: Effects of freezing, growth, and ice cover on gas transport processes in laboratory seawater experiments, Geophys. Res. Lett., 36, L05603, doi:10.1029/2008GL036318, 2009.

Lueker, T. J., Dickson, A. G., and Keeling, C. D.: Ocean pCO_2 calculated from dissolved inorganic carbon, alkalinity, and equations for K1 and K2: validation based

on laboratory measurements of CO_2 in gas and seawater at equilibrium, Mar. Chem., 70, 105–119, 2000.

Manizza, M., Follows, M. J., Dutkiewicz, S., Menemenlis, D., McClelland, J. W., Hill, C. N., Peterson, B. J., and R. M. Key: A model of the Arctic Ocean carbon cycle, J. Geophys. Res., 116, C12020, doi:10.1029/2011JC006998, 2011.

Maréchal, D., A soil-based approach to rainfall-runoff modelling in ungauged catchments for England and Wales. PhD thesis, Cranfield University, U.K., 157 pp, 2004.

Maritorena, S., d'Andon, O. H. F., Mangin, A., and Siegel, D. A.: Merged satellite ocean color data products using a bio-optical model: Characteristics, benefits and issues, Remote Sensing of Environment, 114, 1791-1804, doi:10.1016/j.rse.2010.04.002, 2010.

Matsuoka, A., Huot, Y., Shimada, K., Saitoh, S., and Babin, M.: Bio-optical characteristics of the western Arctic Ocean: Implications for ocean color algorithms, Canadian J. Remote Sens., 33, 503–518, doi:10.5589/m07-059, 2007.

Meier, W., Fetterer, F., Savoie, M., Mallory, S., Duerr, R., and Stroeve, J.: NOAA/NSIDC Climate Data Record of Passive Microwave Sea Ice Concentration. Version 2, Boulder, Colorado USA: National Snow and Ice Data Center,

http://dx.doi.org/10.7265/N55M63M1, 2013.

Moore, T. S., Dowell, M. D., and Franz, B. A.: Detection of coccolithophore blooms in ocean color satellite imagery: A generalized approach for use with multiple sensors, Rem. Sens. Env., 117, 249–263, doi: 10.1016/j.rse.2011.10.001, 2012.

Mucci, A., Lansard, B., Miller, L. A., and Papakyriakou, T. N.: CO_2 fluxes across the air-sea interface in the southeastern Beaufort Sea: Ice-free period, J. Geophys. Res., 115, C04003, doi:10.1029/2009JC005330, 2010.

Murata, A.: Increased surface seawater pCO_2 in the eastern Bering Sea shelf: An effect of blooms of coccolithophorid *Emiliania huxleyi*? Global Biogeochem. Cycles, 20, GB4006, doi:10.1029/2005GB002615, 2006.

Murray, F. W.: On the computation of saturation vapor pressure. J. Applied Meteorology, 6, 203–204, 1967.

Nakaoka, S., Telszewski, M., Nojiri, Y., Yasunaka, S., Miyazaki, C., Mukai, H., and Usui, N.: Estimating temporal and spatial variation of sea surface pCO_2 in the North Pacific using a self organizing map neural network technique, Biogeosciences, 10, 6093-6106, doi:10.5194/bg-10-6093-2013, 2013.

Olsen, A., Brown, K. R., Chierici, M., Johannessen, T., and Neill, C.: Sea-surface CO_2 fugacity in the subpolar North Atlantic, Biogeosciences, 5, 535–547,

doi:10.5194/bg-5-535-2008, 2008.

Olsen, A., Key, R. M., van Heuven, S., Lauvset, S. K., Velo, A., Lin, X., Schirnick, C., Kozyr, A., Tanhua, T., Hoppema, M., Jutterström, S., Steinfeldt, R., Jeansson, E., Ishii, M., Pérez, F. F., and Suzuki, T.: The Global Ocean Data Analysis Project version 2 (GLODAPv2) – an internally consistent data product for the world ocean, Earth Syst. Sci. Data, 8, 297–323, 2016, doi:10.5194/essd-8-297-2016, 2016.

O'Reilly, J. E., Maritorena, S., Mitchell, B. G., Siegel, D. A., Carder, K. L., Garver, S. A., Kahru, M., and McClain, C.: Ocean color chlorophyll algorithms for SeaWiFS, J. Geophys. Res., 103, 24937–24953, doi:10.1029/98JC02160, 1998.

Peng, G., Meier, W., Scott, D., and Savoie, M.: A long-term and reproducible passive microwave sea ice concentration data record for climate studies and monitoring. Earth Syst. Sci. Data 5: 311–318, http://dx.doi.org/10.5194/essd-5-311-2013, 2013.

Perrette, M., Yool, A., Quartly, G. D., and Popova, E. E.: Near-ubiquity of ice-edge blooms in the Arctic, Biogeosciences, 8, 515–524, doi:10.5194/bg-8-515-2011, 2011.

Popova, E. E., Yool, A., Coward, A. C., Dupont, F., Deal, C., Elliott, S., Hunke, E., Jin, M., Steele, M., and Zhang, J., What controls primary production in the Arctic Ocean? Results from an intercomparison of five general circulation models with biogeochemistry, J. Geophys. Res., 117, C00D12, doi:10.1029/2011JC007112, 2012.

Reynolds, R. W., Rayner, N. A., Smith, T. M., Stokes, D. C., and Wang, W.: An improved in situ and satellite SST analysis for climate, J. Climate, 15, 1609–1625, 2002.

Schuster, U., McKinley, G. A., Bates, N., Chevallier, F., Doney, S. C., Fay, A. R., González-Dávila, M., Gruber, N., Jones, S., Krijnen, J., Landschützer, P., Lefèvre, N., Manizza, M., Mathis, J., Metzl, N., Olsen, A., Rios, A. F., Rödenbeck, C., Santana-Casiano, J. M., Takahashi, T., Wanninkhof, R., and Watson, A. J.: An assessment of the Atlantic and Arctic sea–air CO_2 fluxes, 1990–2009, Biogeosciences, 10, 607–627, doi:10.5194/bg-10-607-2013, 2013.

Shutler, J. D., Land, P. E., Brown, C. W., Findlay, H. S., Donlon, C. J., Medland, M., Snooke, R., and Blackford, J. C.: Coccolithophore surface distributions in the North Atlantic and their modulation of the air-sea flux of CO_2 from 10 years of satellite Earth observation data, Biogeosciences, 10, 2699–2709, doi:10.5194/bg-10-2699-2013, 2013

Semiletov, I., Makshtas, A., Akasofu, S.-I., and Andreas, E. L: Atmospheric CO_2 balance: The role of Arctic sea ice, Geophys. Res. Lett., 31, L05121, doi:10.1029/2003GL017996, 2004.

Semiletov, I. P., Pipko, I. I., Repina, I., and Shakhova, N. E.: Carbonate chemistry

dynamics and carbon dioxide fluxes across the atmosphere–ice–water interfaces in the Arctic Ocean: Pacific sector of the Arctic, J. Mar. Syst., 66, 204–226, doi:10.1016/j.jmarsys.2006.05.012, 2007.

Signorini, S. R., and McClain, C. R.: Effect of uncertainties in climatologic wind, ocean pCO_2, and gas transfer algorithms on the estimate of global sea-air CO_2 flux, Global Biogeochem. Cycles, 23, GB2025, doi:10.1029/2008GB003246, 2009.

Siswanto, E., Tang, J., Ahn, Y.-H., Ishizaka, J., Yoo, S., Kim, S.-W., Kiyomoto, Y., Yamada, K., Chiang, C., and Kawamura, H.: Empirical ocean color algorithms to retrieve chlorophyll-a, total suspended matter, and colored dissolved organic matter absorption coefficient in the Yellow and East China Seas, J. Oceanogr., doi:10.1007/s10872-011-0062-z, 2011.

Siswanto, E., Ishizaka, J., Tripathy, S. C., and Miyamura, K.: Detection of harmful algal blooms of *Karenia mikimotoi* using MODIS measurements: a case study of Seto-Inland Sea, Japan, Remote Sensing of Environment, 129, 185–196, doi:10.1016/j.rse.2012.11.003, 2013.

Smyth, T. J., Tyrrell, T., Tarrant, B.: Time series of coccolithophore activity in the Barents Sea, from twenty years of satellite imagery, Geophys. Res. Lett., 31, L11302, doi:10.1029/2004GL019735, 2004.

Steele, M., Morley, R., and Ermold, W.: PHC: A global ocean hydrography with a high quality Arctic Ocean, J. Climate, 14, 2079–2087, 2001.

Sweeney, C., Gloor, E., Jacobson, A. R., Key, R. M., McKinley, G., Sarmiento, J. L., and Wanninkhof, R.: Constraining global air-sea gas exchange for CO_2 with recent bomb ^{14}C measurements, Global Biogeochem. Cycles, 21, GB2015, doi:10.1029/2006GB002784, 2007.

Takahashi, T., Sutherland, S. C., Wanninkhof, R., Sweeney, C., Feely, R. A., Chipman, D. W., Hales, B., Friederich, G., Chavez, F., Sabine, C., Watson, A., Bakker, D. C. E., Schuster, U., Metzl, N., Yoshikawa-Inoue, H., Ishii, M., Midorikawa, T., Nojiri, Y., Körtzinger, A., Steinhoff, T., Hoppema, M., Olafsson, J., Arnarson, T. S., Tilbrook, B., Johannessen, T., Olsen, A., Bellerby, R., Wong, C. S., Delille, B., Bates, N. R., de Baar, H. J. W.: Climatological mean and decadal changes in surface ocean pCO_2, and net sea-air CO_2 flux over the global oceans. Deep-Sea Res. II, 56, 554–577, 2009.

Takahashi, T., Sutherland, S.C., and Kozyr, A.: Global Ocean Surface Water Partial Pressure of CO_2 Database: Measurements Performed During 1957–2014 (Version 2014). ORNL/CDIAC-160, NDP-088(V2014). Carbon Dioxide Information Analysis Center, Oak Ridge National Laboratory, U.S. Department of Energy, Oak Ridge, Tennessee, doi: 10.3334/CDIAC/OTG.NDP088(V2014), 2015.

Tassan, S.: Local algorithms using SeaWiFS data for the retrieval of phytoplankton, pigments, suspended sediment, and yellow substance in coastal waters, Applied Opt., 33, 2369–2378, doi:10.1364/AO.33.002369, 1994.

Telszewski, M., Chazottes, A., Schuster, U., Watson, A. J., Moulin, C., Bakker, D.C.E., González-Dávila, M., Johannessen, T., Körtzinger, A., Lüger, H., Olsen, A., Omar, A., Padin, X. A., Ríos, A. F., Steinhoff, T., Santana-Casiano, M., Wallace, D. W. R., and Wanninkhof, R.: Estimating the monthly pCO_2 distribution in the North Atlantic using a self-organizing neural network, Biogeosciences, 6, 1405–1421, doi:10.5194/bg-6-1405-2009, 2009.

Ulfsbo, A., Cassar, N., Korhonen, M., van Heuven, S., Hoppema, M., Kattner, G., and G. Anderson, L.: Late summer net community production in the central Arctic Ocean using multiple approaches, Global Biogeochem. Cycles, 28, 1129–1148, doi:10.1002/2014GB004833, 2014.

van Heuven, S., Pierrot, D., Lewis, E., and Wallace, D. W. R.: MATLAB Program Developed for CO2 System Calculations, ORNL/CDIAC-105b. Carbon Dioxide Information Analysis Center, Oak Ridge National Laboratory, US Department of Energy, Oak Ridge, Tennessee, 2009.

Wanninkhof, R.: Relationship between wind speed and gas exchange over the ocean, J.

Geophys. Res., 97(C5), 7373–7382, doi:10.1029/92JC00188, 1992.

Wanninkhof, R., Park, G. -H., Takahashi, T., Sweeney, C., Feely, R., Nojiri, Y., Gruber, N., Doney, S. C., McKinley, G. A., Lenton, A., Le Quéré, C., Heinze, C., Schwinger, J., Graven, H., and Khatiwala, S.: Global ocean carbon uptake: magnitude, variability and trends, Biogeosciences, 10, 1983–2000, doi:10.5194/bg-10-1983-2013, 2013.

Wanninkhof, R.: Relationship between wind speed and gas exchange over the ocean revisited, Limnol. Oceanogr.: Methods, 12, 351-362, 2014.

Weiss, R. F.: Carbon dioxide in water and seawater: the solubility of a non-ideal gas, Mar. Chem., 2, 203–215, 1974.

Yasunaka, S., Nojiri, Y., Nakaoka, S., Ono, T., Whitney, F. A., and Telszewski, M.: Mapping of sea surface nutrients in the North Pacific: Basin-wide distribution and seasonal to interannual variability, J. Geophys. Res. Oceans, 119, 7756–7771, doi:10.1002/2014JC010318, 2014.

Yasunaka, S., Murata, A., Watanabe, E., Chierici, M., Fransson, A., van Heuven, S., Hoppema, M., Ishii, M., Johannessen, T., Kosugi, N., Lauvset, S. K., Mathis, J. T., Nishino, S., Omar, A. M., Olsen, A., Sasano, D., Takahashi, T., and Wanninkhof, R.: Mapping of the air–sea CO_2 flux in the Arctic Ocean and its adjacent seas: basin-wide distribution and seasonal to interannual variability, Polar Science, 10,

323–334, doi:10.1016/j.polar.2016.03.006, 2016.

Figure 1: Map of the Arctic Ocean and its adjacent seas. Gray contour lines show the 1000, 2000, 3000, and 4000 m isobaths. Blue lines show the 17-year annual mean position of the ice edge (SIC = 15 %). Area for the mapping is north of 60° N (heavy black circle). Sectors selected for regional analysis are the Arctic Ocean (dashed magenta line), the Greenland/Norwegian Seas (green 1), the Barents Sea (green 2), and the Chukchi Sea (green 3).

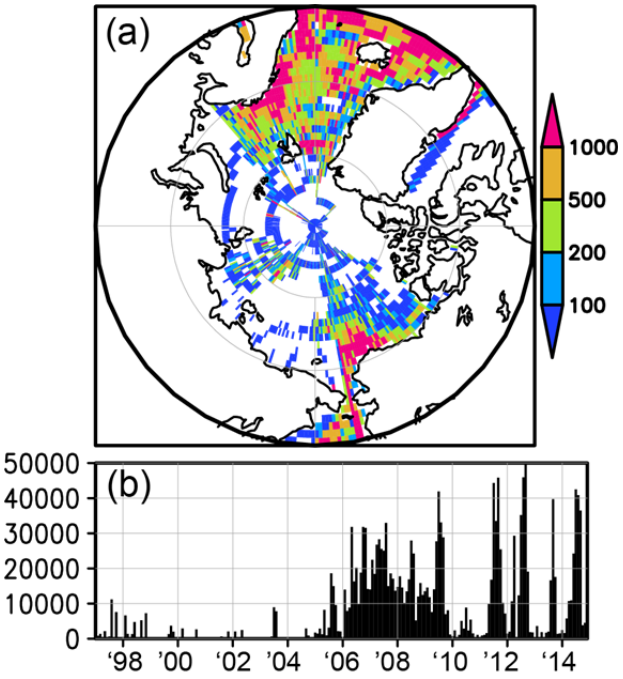

Figure 2: (a) The number of ocean surface CO_2 data in the grid boxes (1° × 1°) used in this study. Data are from SOCATv4, LDEOv2014, GLODAPv2, and collected by R/V *Mirai* of JAMSTEC between 1997 and 2014. (b) Monthly number of CO_2 data in the analysis area (north of 60° N) from 1997 to 2014.

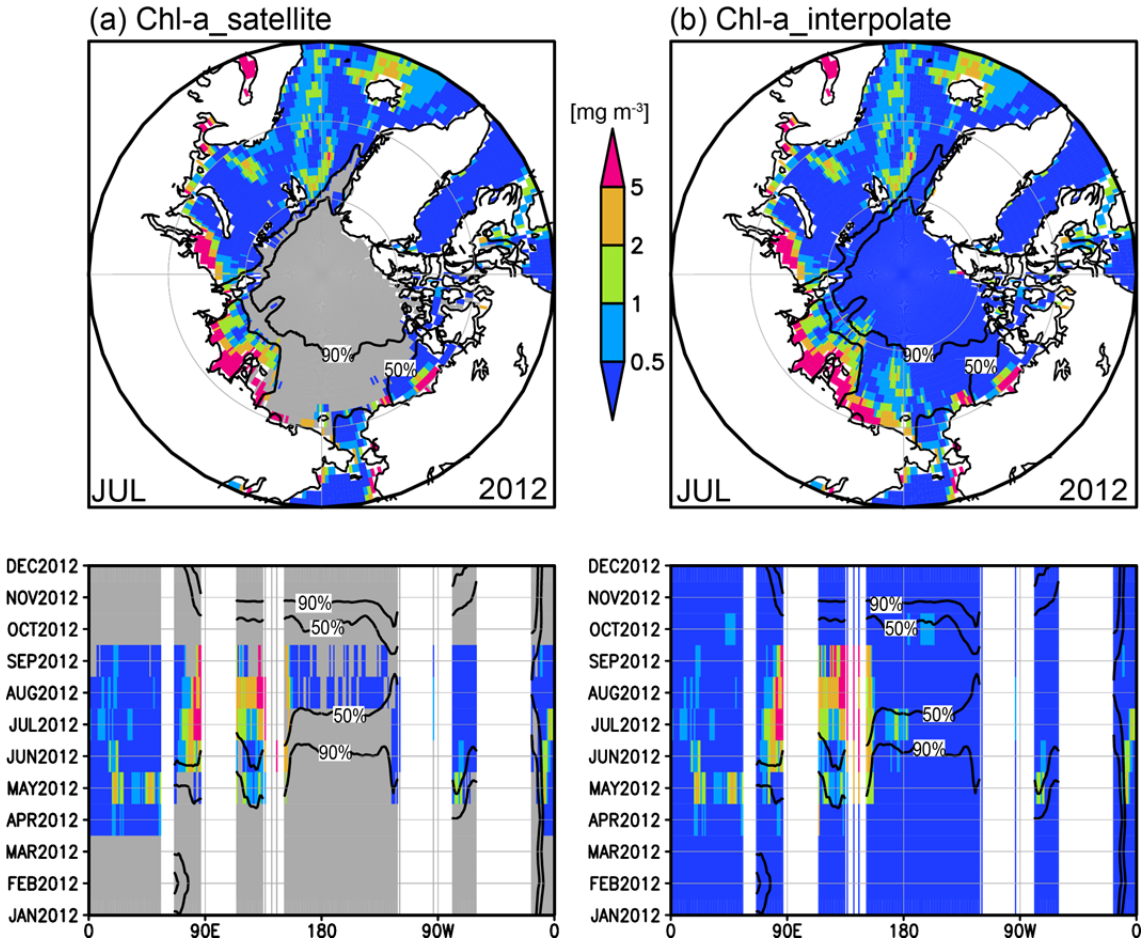

Figure 3: (a) Original and (b) interpolated Chl-a [mg m^{-3}] in July 2012 (upper panels), and along 75°N in 2012 (lower panels). Black lines denote SIC of 50% and 90%. Gray areas in (a) indicate missing Chl-a data.

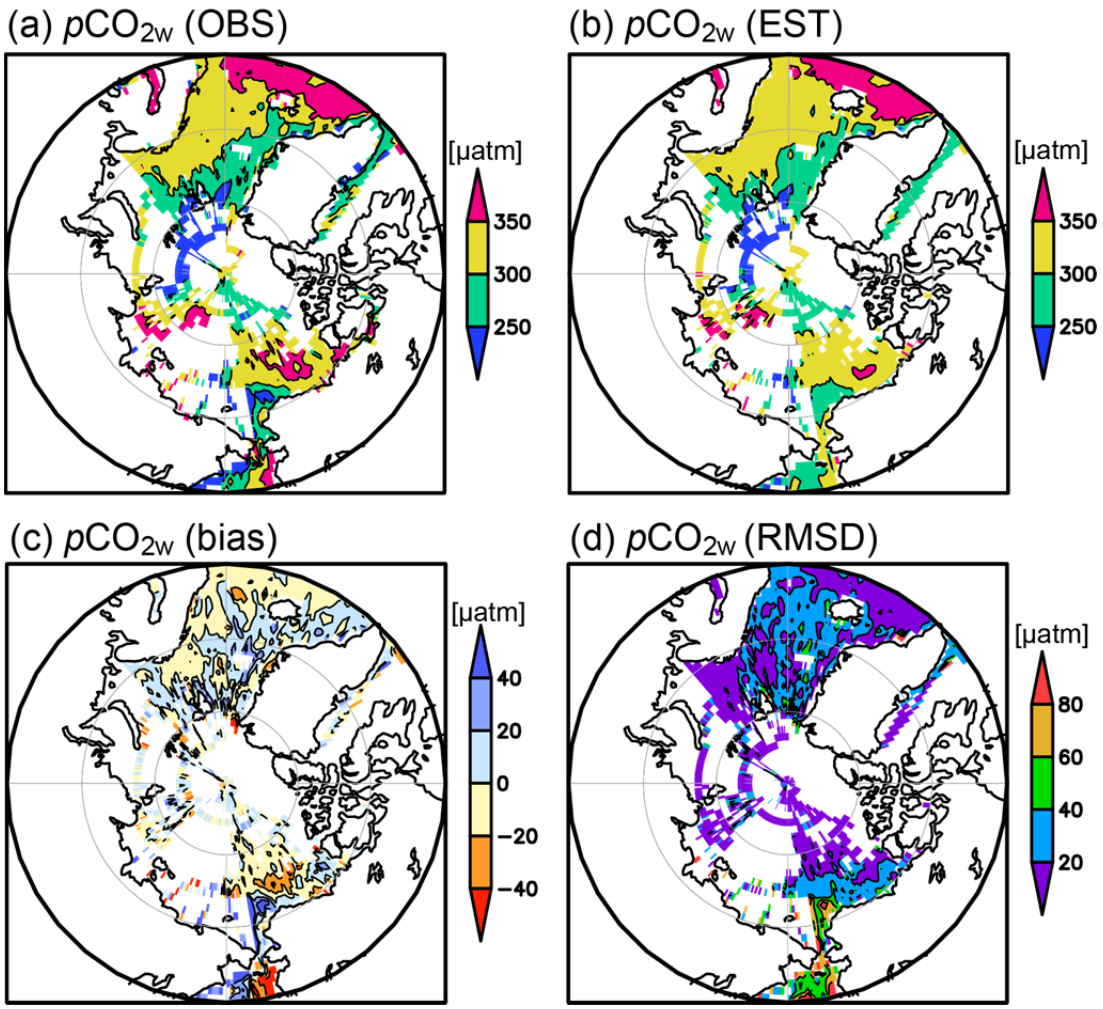

Figure 4: (a) Observed pCO_{2w} averaged over the whole analysis period [µatm]. (b) Estimated pCO_{2w} averaged over the grid boxes in which observed pCO_{2w} values were available [µatm]. (c) Bias (estimate–observation) and (d) root-mean-square-difference between observed and estimated pCO_{2w} averaged over the whole analysis period [µatm].

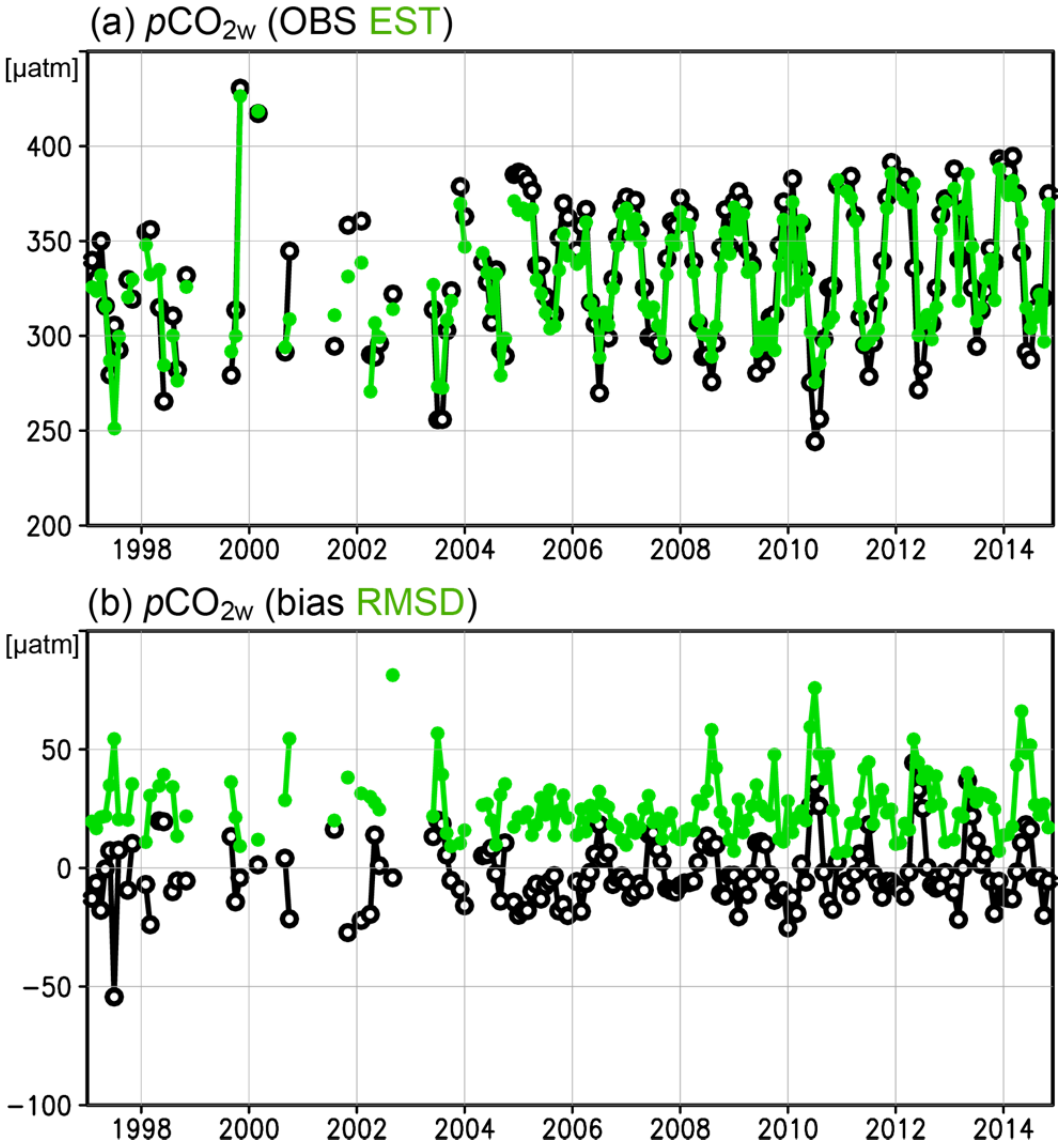

Figure 5: (a) Monthly time series of observed pCO_{2w} averaged over the entire analysis area (black), and estimated pCO_{2w} averaged over the grid boxes in which observed pCO_{2w} values were available (green) [µatm]. (b) Bias (estimate–observation; black) and root-mean-square-difference (green) between observed and estimated pCO_{2w} averaged over the entire analysis area [µatm].

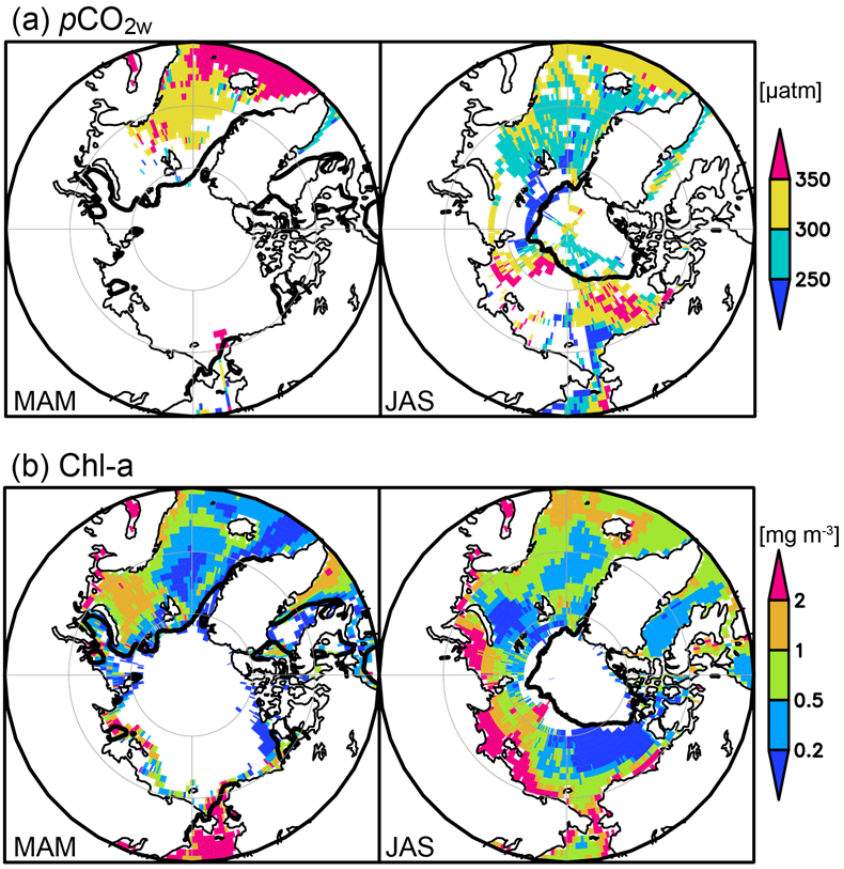

Figure 6: (a) Observed pCO_{2w} [µatm], and (b) non-interpolated Chl-a [mg m^{-3}] in March–May (left), and July–September (right) from 1997 to 2014.

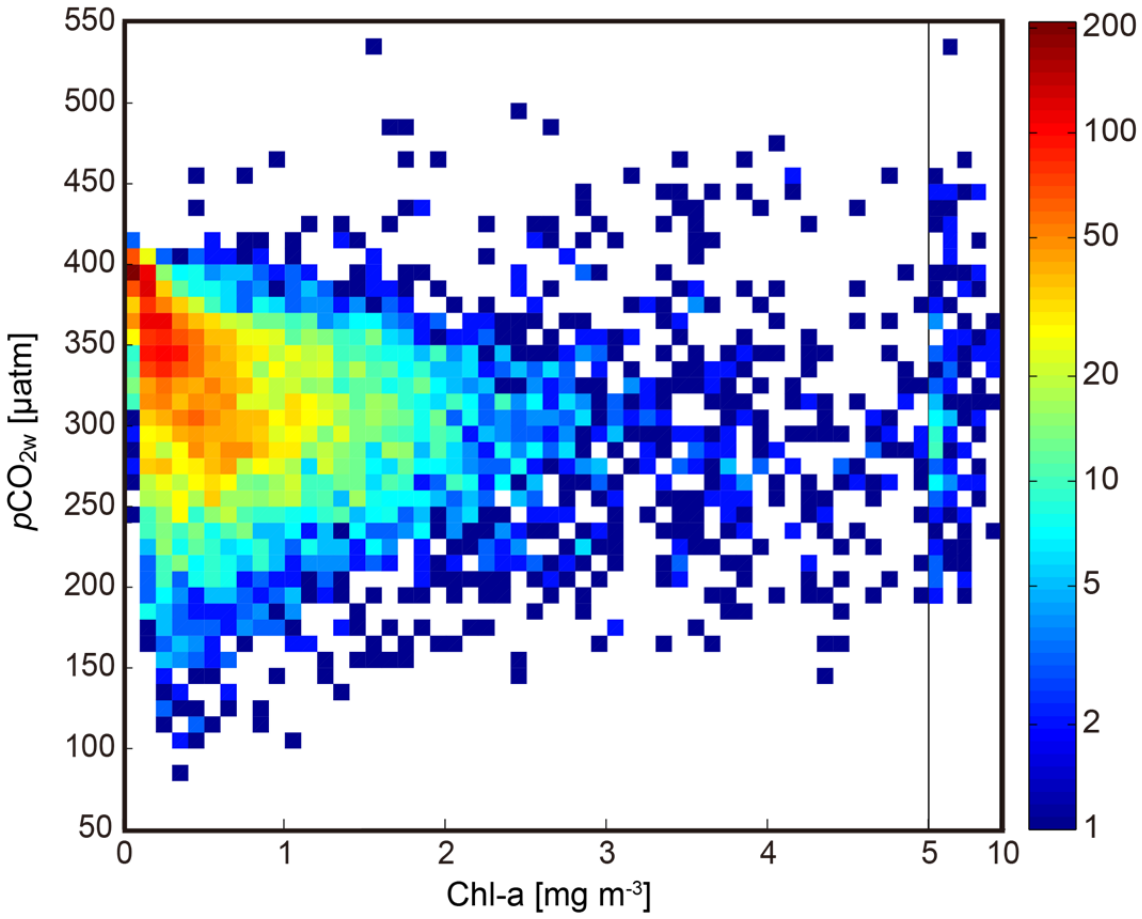

Figure 7: Observed pCO_{2w} [µatm] vs. satellite Chl-a [mg m^{-3}] in the Arctic Ocean and its adjacent seas (north of 60° N) from 1997 to 2014. Colors indicate the number of data pairs in a 0.1 mg m^{-3} × 5 µatm bin when Chl-a ≤ 5 mg m^{-3}, or in a 1 mg m^{-3} × 5 µatm bin when Chl-a > 5 mg m^{-3}.

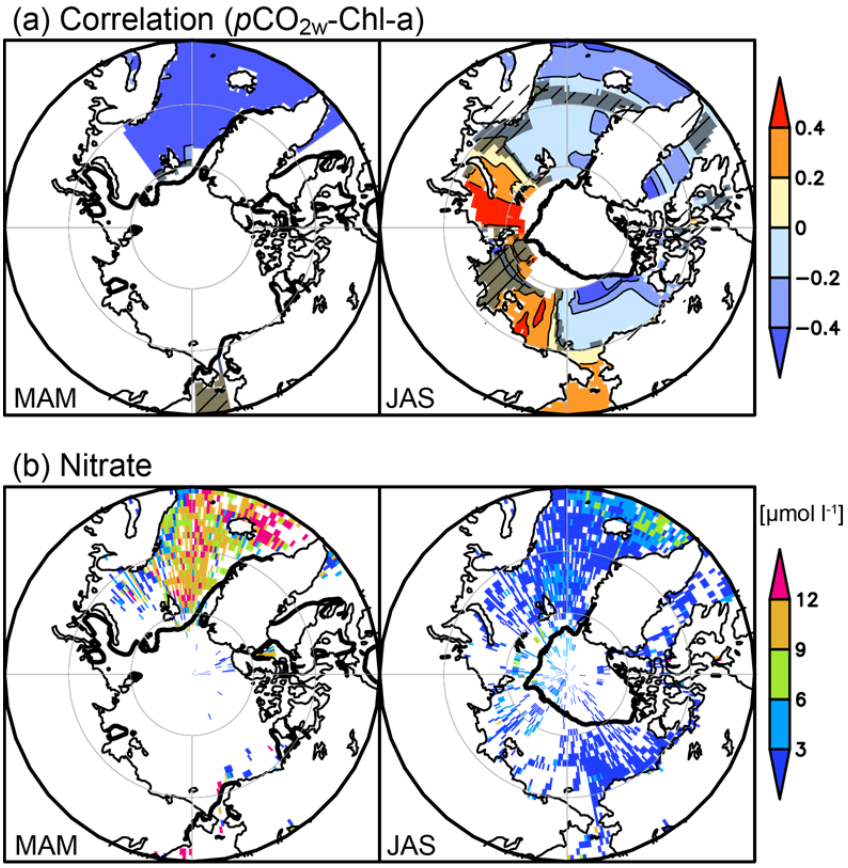

Figure 8: (a) Spatial correlation (correlation coefficient, r) between pCO_{2w} and Chl-a in a window size of ±1 month, ±5° of latitude, and ±30° of longitude in March–May (left), and July–September (right). Darker hatched areas represent values in grids where correlations are insignificant ($P > 0.05$). (b) Surface nitrate concentration [µmol l^{-1}] in March–May (left), and July–September (right) from 1997 to 2014.

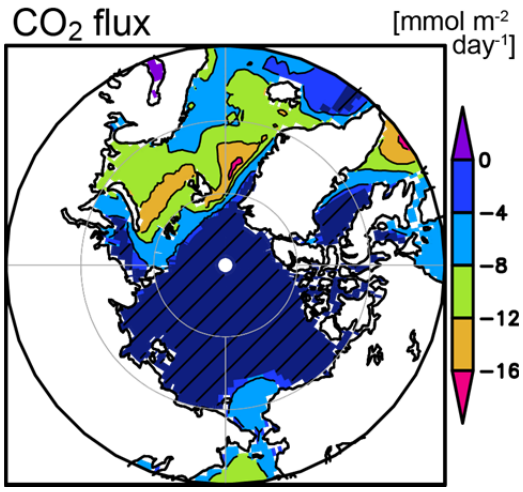

Figure 9: Eighteen-year annual means of CO_2 flux [mmol m^{-2} day^{-1}] (negative values indicate flux into the ocean). Darker hatched areas represent show values in grids where fluxes were smaller than the uncertainty, estimated as described in the text.

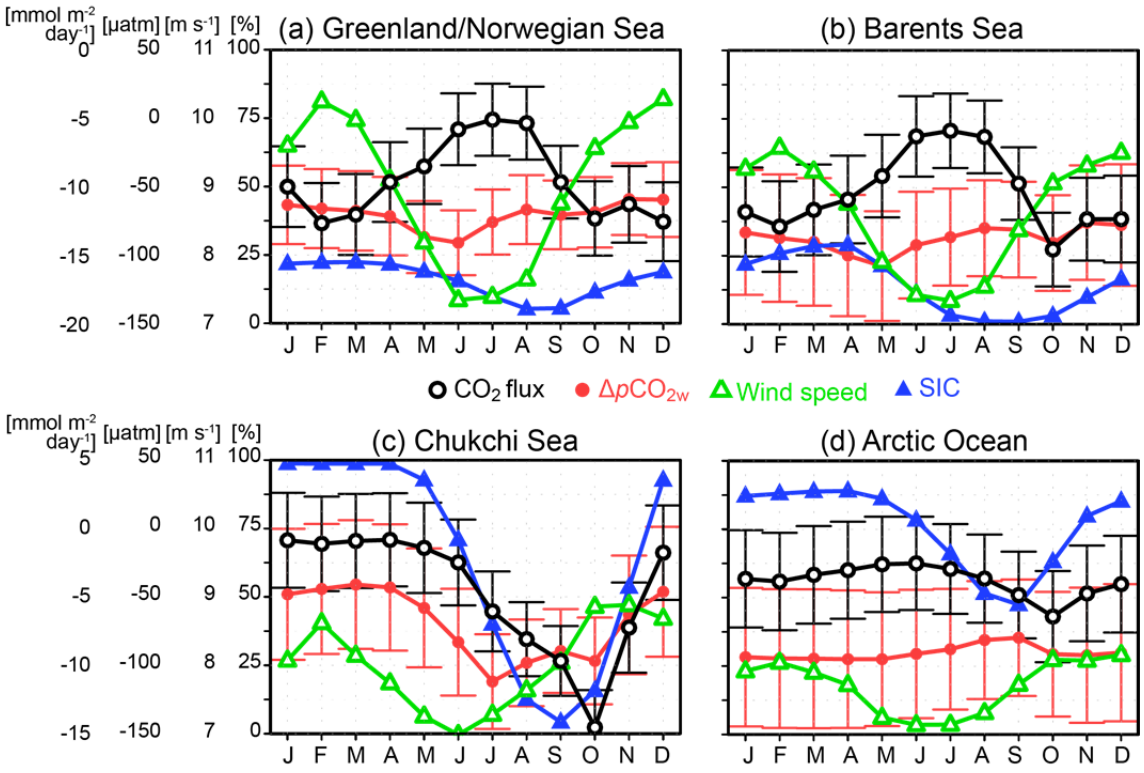

Figure 10: Eighteen-year monthly mean CO_2 flux [mmol m^{-2} day^{-1}] (black), ΔpCO_2 [µatm] (red), wind speed [m sec^{-1}] (green), and SIC [%] (blue), averaged over (a) the Greenland/Norwegian Seas, (b) the Barents Sea, (c) the Chukchi Sea, and (d) the Arctic Ocean. Error bars indicate the uncertainty.

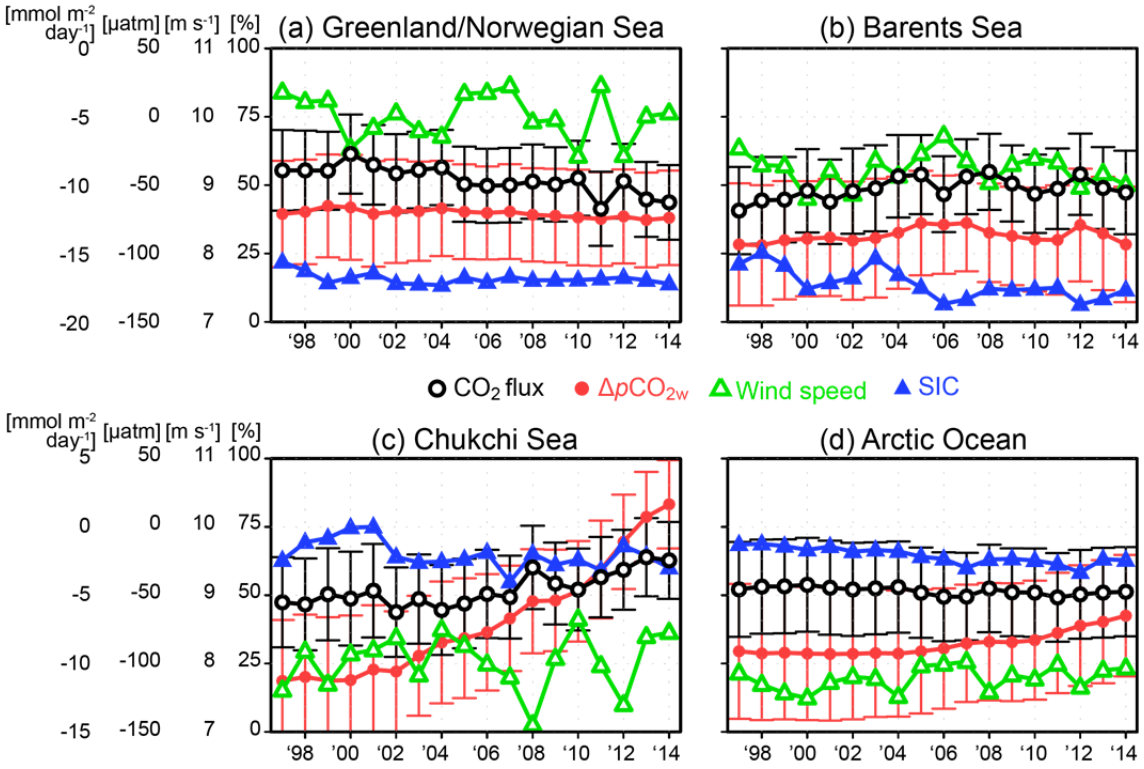

Figure 11: Area-mean interannual variations of CO_2 flux [mmol m^{-2} day^{-1}] (black), ΔpCO_2 [µatm] (red), wind speed [m sec^{-1}] (green), and SIC [%] (blue) in (a) the Greenland/Norwegian Seas, (b) the Barents Sea, (c) the Chukchi Sea, and (d) the Arctic Ocean. Error bars indicate the uncertainty.

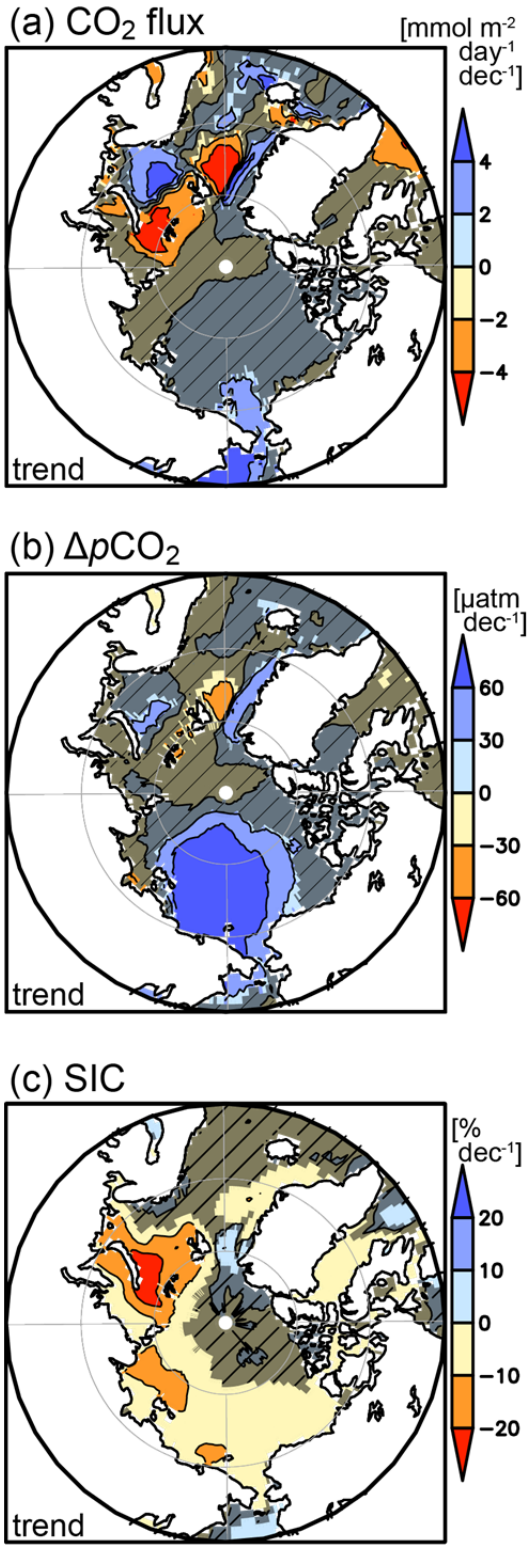

Figure 12: Trends in (a) CO_2 flux [mmol m^{-2} day^{-1} $decade^{-1}$], (b) ΔpCO_2 [µatm $decade^{-1}$], and (c) SIC [% $decade^{-1}$]. Darker hatched areas represent values in grids where trend values were less than the uncertainty, estimated as described in the text.

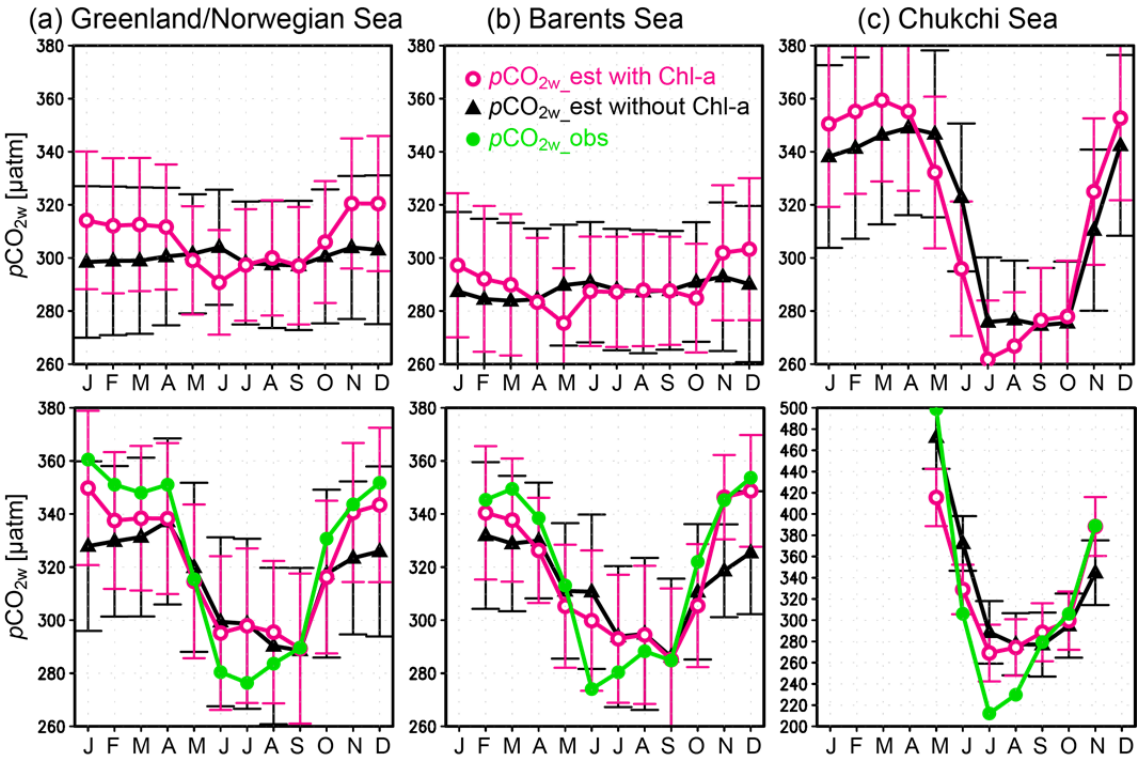

Figure 13: Eighteen-year averaged pCO_{2w} seasonal variations [µatm] in (a) the Greenland/Norwegian Seas, (b) the Barents Sea, and (c) the Chukchi Sea. Black lines with triangles show estimates without Chl-a; magenta lines with open circles show estimates with Chl-a; green lines with closed circles show observed values. The upper panels show pCO_{2w} averaged for all grid cells with each region, and the lower panels show pCO_{2w} averaged over the grid boxes in which observed pCO_{2w} values were available. Error bars show the uncertainty, estimated as described in the text.

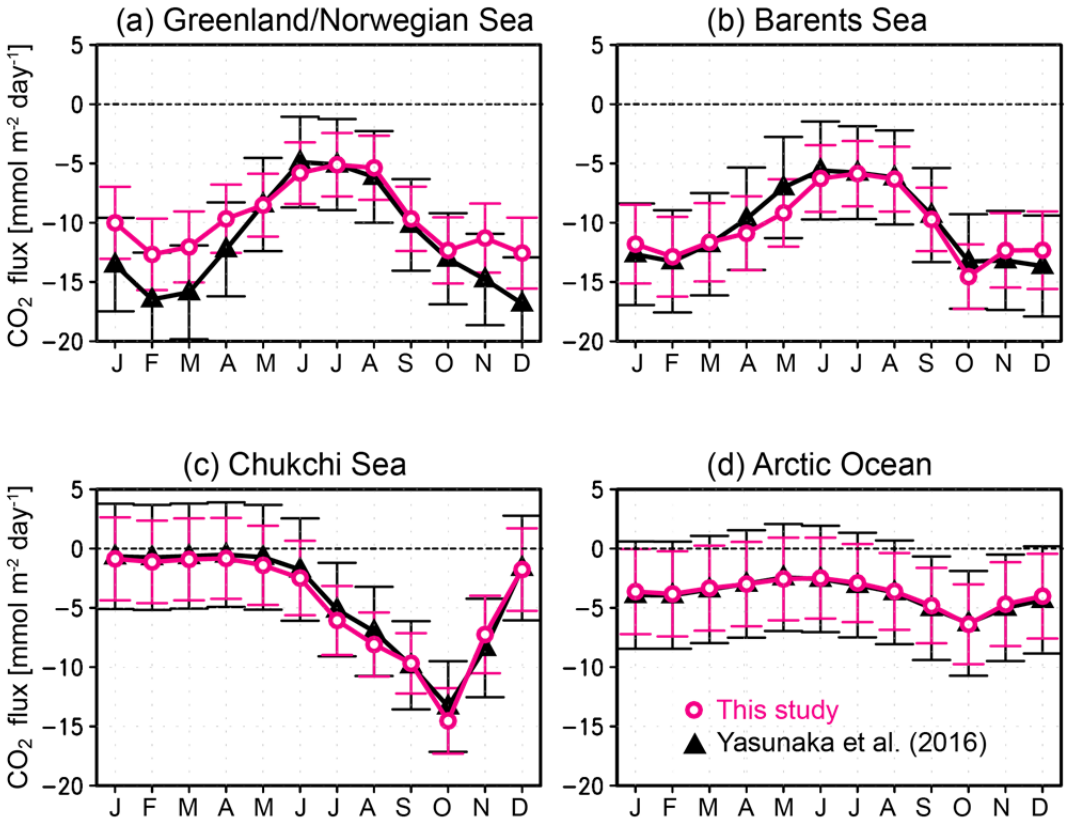

Figure 14: Eighteen-year monthly mean CO_2 flux [mmol m^{-2} day^{-1}] averaged over (a) the Greenland/Norwegian Seas, (b) the Barents Sea, (c) the Chukchi Sea, and (d) the Arctic Ocean. Black lines with triangles show estimates without Chl-a by Yasunaka et al. (2016); magenta lines with open circles show estimates with Chl-a. Error bars show the uncertainty, estimated as described in the text.

Table 1: RMSD [mg m^{-3}] and correlation (r) between Chl-a values

	standard algorithm		coastal algorithm	
	RMSD	r	RMSD	r
Chl-a from Arctic algorithm	0.80	0.90	0.81	0.87
Interpolated Chl-a from Arctic algorithm	0.37	0.92	0.48	0.86